Communication-Navigation Integrated Satellite Constellation for Lunar Exploration: Frozen-Orbit Based HyInc Walker

Guoquan Chen, *Graduate Student Member, IEEE*, Shaohua Wu, *Member, IEEE*, Junhua You, and Qinyu Zhang, *Senior Member, IEEE*

***Abstract*—Deep space communication systems play a key role in human endeavors for lunar basing, Mars, and further cosmic exploration. In pursuit of establishing the Moon as a deep space Internet portal for future human exploration, a lunar communication and navigation integrated (CNI) satellite constellation design is intended into consideration. Based on Fibonacci lattice virtual observation point model, featuring better uniformity and stochasticity, we derive objectives related to access coverage, power, quadruple coverage, and geometric dilution of precision (GDOP), together with multiple multi-objective optimization problems (MOPs) combined with Earth-Moon difference analysis to explore better utilization of overall resources in the lunar integrated constellation. The pareto model, non-dominated sorting genetic algorithm-II (NSGA-II), and the construction of the constellation system are incorporated into the solution to pursue a higher guiding value. In particular, inspired by the lunar frozen orbit (LFO), the hybrid inclination (HyInc) Walker configuration is proposed with theoretical validation and simulation evaluation, showing some superiority over traditional Walker and remains generalizable. Extensive simulation and comprehensive analysis are performed, including the pareto-optimal integrated constellations and the revelation of HyInc Walker's coverage equalization capability, with the latter being less studied. The entire constellation design process of this work is highly migratory and the proposed perspective of the configuration is enlightening.**

***Index Terms*—Integrated satellite constellation design, lunar frozen orbit, HyInc Walker, MOP, NSGA-II.**

I. Introduction

HUMANITY is entering a new era of lunar exploration and development, with more and more unmanned probes and manned spacecrafts scheduled on the Moon [1]. Following the *Apollo* program of the last century, the United States announced the second Moon landing program, *Artemis*, in 2017, and as of October 2023, 29 countries, including Germany, Canada, Japan, Brazil, *etc.*, have signed the *Artemis* Accords. And alongside NASA, on the ESA's part, more than the *Moonlight* initiative [2], it has also signed a contract with rocket maker *ArianeGroup* and plans to land and build a base on the Moon by 2025 so as to exploit the lunar resources. In this new round of space exploration, India [3] and China [4] are also proactively involved in propelling, with the latter pioneering the strategic vision of lunar antarctic exploration and having successfully completed five lunar exploration missions [5]. Hence for now, based on the background that aerospace is now in full swing to promote the current explosive development of deep space communication worldwide, considering numerous manned lunar landing programs in the next decade, as well as the future communication and navigation demands of lunar bases (such as *Artemis* Base Camp and ESA Base Camp) and lunar surface users, the early lunar halo orbit (LHO)-based relay satellite (SAT) such as *Queqiao* 1st relay SAT [6] can no longer support, and the construction of lunar SAT constellation (CON) networks has become increasingly necessary. Besides, considering that CNSA has also commenced the 4th phase program of lunar exploration and the validation of the *Queqiao Constellation*, where the latter aims to compose a circumlunar integrated CON to support lunar scientific research and surface users' demands, and to expand into a lunar-centered deep space Internet [7] in the future and grow towards an ambitious portal for human exploration of Mars and deep space (as shown in Fig. 1), it is affirmable that the research of circumlunar CON network is of great precursor and foundational.

Being the first and one of the most crucial stages in CON network construction [8], the design of CON contributes directly to the comprehensive construction cost and overall system performance of the CON network. Presently, regarding the Earth SAT orbit, in the context of 6G space-air-ground-sea integrated network [9], Low Earth Orbit (LEO) SAT [10] are favored by researchers for their low double-hop propagation delay, and in spite of frequent handover challenges [11], they perform optimally in high-capacity services [12] and time-sensitive services due to low altitude, with the CON networks typified by giant low-orbit also being thriving [13]. In [14], a mega-CON scheme was proposed to achieve seamless global connectivity and high-rate backhaul transmission for integrated SAT ground networks. In [15], a high-capacity backhaul data services was investigated under terrestrial SAT networks and a LEO-based ultra dense CON [16] solution was proposed to meet the large backhaul capacity requirements of subscribers [17]. And based on stochastic geometry and queuing theory, Wang *et al.* proposed a multi-layer LEO dense CON scheme that takes into account traffic dynamics [18]. Many literatures also considered various aspects of performance analysis and

This work has been supported in part by the National Natural Science Foundation of China under Grant nos. 61831008, 61871147, 62027802, and in part by the Guangdong Basic and Applied Basic Research Foundation under Grant no. 2022B1515120002, and in part by the Major Key Project of PCL under Grant PCL2021A03-1. (*Corresponding authors: Shaohua Wu; Qinyu Zhang.*)

G. Chen and J. You are with the Department of Electronics and Information Engineering, Harbin Institute of Technology (Shenzhen), Shenzhen 518055, China (e-mail: 180210217@stu.hit.edu.cn; youjunhua@stu.hit.edu.cn).

S. Wu and Q. Zhang are with the Guangdong Provincial Key Laboratory of Aerospace Communication and Networking Technology, Harbin Institute of Technology (Shenzhen), Shenzhen 518055, China, and also with the Peng Cheng Laboratory, Shenzhen 518055, China (e-mail: hitwush@hit.edu.cn; zqy@hit.edu.cn).

optimization based on the context of mega-CON networks, such as resource allocation [19], backhaul capacity [20], link interference [21], coverage [22], latency [23], *etc*.

However, while the mega-CON scheme could be a straightforward crude solution to the multiple performance requirements sought by integrated CON designs, it is extravagant for the Moon, as mega-CON involves extremely high space segment cost[1] [24]. Considering the launch cost solely, owing to the 2nd cosmic velocity restraint, the launch cost of circumlunar orbit SAT is already dozens to hundreds times higher that of Earth orbit SAT [25]. Therefore, optimization and performance squeezing for CON configuration are more demanding in the lunar CON construction. In [26], the authors modeled and optimized resource-constrained sparse IoT CON and designed a quasi-optimal coverage topology. Similarly, there are some studies on optimizing communication CON in terms of coverage maximization [27] or SAT number minimization [28]. While [29] proposed a LEO-based navigation CON design scheme oriented to dilution of precision (DOP) metrics, and [30] investigated multi-objective CON design for GNSS reflectometry mission with evolutionary algorithm [27]. The work [31] examined the possibility of navigation augmentation based on LEO communication CONs. The work [32] investigated the feasibility of weak Earth GNSS signals for lunar exploration based on the demand of ESA's lunar navigation program. Different from [32], considering the limitation of Earth GNSS signals for lunar navigation in terms of DOP, the works [33]–[38] both focus on the design of lunar-specific GNSS CONs. Most of researchers, including Murata *et al.*, focused on the navigation coverage of lunar South Pole [35], [36], and specifically, Murata *et al.* conducted a performance analysis in the context of the JAXA-planned lunar navigation CON. While Bhamidipati *et al.* proposed a lunar navigation CON scheme using GPS signals for time transfer [37], [38].

Nevertheless, existing researches on CON optimization focused primarily on modeling of single mission requirement [39], [40], *i.e.*, communication or navigation missions. Few researches that considered multi-objective optimization problem (MOP) resorted to choose the simpler but less adaptable linear weighted model [41] and ϵ-constraint model [14] due to the complexity of the CON design problem, which essentially still transformed the MOP into single-objective optimization problem (SOP) for simplified solution at the cost of reduced guiding significance. To our best knowledge, integrated CON design efforts in the context of communication and navigation integrated (CNI) [42] are relatively lacking [43]–[46]. Among them, the work [43] directly evaluated the navigation performance by using only the accessible SAT numbers overhead, ignoring the optimization of the CON's geometry. The work [44] investigated the potential implementation of lunar-specific communication and navigation services for the landing requirements of the ESA's future lunar lander, yet only focused on the lunar South Pole coverage as in the case of [45], [46].

Thus in pursuit of the future vision of space communication and to address the above issues, in this paper, we aim to investigate a lunar integrated CON design for multiple objectives related to access coverage, power, quadruple coverage, and geometric dilution of precision (GDOP). The following aspects are considered. *First*, considering that the commonly used traditional configurations such as Walker[2] [47] and Flower [48] have made a lot of parameter restrictions for the simplicity and universality of CON design and deployment, such as uniform altitude and uniform orbital inclination [49], which reduce CON diversity and fail to cope with the lunar integrated CON's multiple requirements, the development and analysis of certain new CON configurations will be considered and advocated. *Second*, solving models for MOP with robust adaptability and modern optimization algorithms will be prioritized for focus and adopted to ensure the practicability of our model. *Third*, apart from the rigorous mathematical analysis, the construction of the CON simulation system and the associated visualization of this work is also emphasized. Partial works without focusing on the construction of CON simulation system [18], [50], however, it can assist in identifying problems that are troublesome to obtain through mathematical analysis, while also attracting and advancing researchers interested in the field. Although this could be more costly in terms of funds, time, and efforts, it enhances the instructive value of the research. The specific contributions can be summarized below:

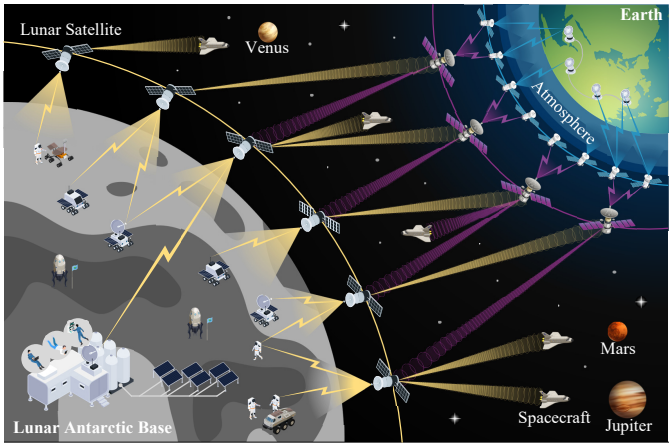

Fig. 1. Lunar antarctic base and the future portal vision.

- We explore the pareto-optimal design of lunar CNI CON in lunar frozen orbit (LFO) space with low latency, based on the difference analysis of Earth-Moon CON construction, including user distribution, gravity model, and channel aspect. This is an important topic oriented to lunar exploration, and related research work on lunar integrated CON is relatively lacking.
- We develop three MOPs studies that involved multiple objectives including access coverage, power, quadruple coverage, and GDOP, which contribute to a better analysis and utilization of the CON's overall resources. And the entire design process and thoughts have a certain reference value and are highly migratory, including the selection of virtual user model, the combination of algo-

[1]The cost of CON consists of space segment, ground segment, and terminal cost. The space segment cost mainly includes the development cost and launch cost paid during the construction phase of the CON system.

[2]The traditional Walker configuration can be divided into two types based on the equalization rule of right ascension of ascending node (RAAN), namely Walker Delta and Walker Star, the former being equalized by 360° and the latter being equalized by 180° and can be equated with Rosetee configuration.

rithm and CON simulation construction.

- We propose the intuitively LFO-inspired hybrid inclination (HyInc) Walker configuration, developed from the traditional Walker and remains generalizable. Theoretical analysis and system simulation are combined to validate its superiority over traditional Walker on CON performance, including access coverage, power, quadruple coverage, and GDOP. And the proposed perspective of the configuration is enlightening.
- Extensive simulation and comprehensive numerical results are provided for analysis and evaluation, including, along with the pareto-optimal CONs, the revelation of the global and local coverage equalization capability of the proposed configuration, which is less studied.

The rest of this paper is organized as follows. In Section II, the considered system model is introduced, followed by the proposed configuration detailed in Section III. The mathematical derivation related to the lunar CON design and the proposal of MOPs are given in Section IV. Section V is dedicated to the solution and algorithms. Simulation results are given in Section VI, followed by conclusions in Section VII.

II. System Model

In this section, we propose the global virtual observation point (VOP) model to represent the virtual lunar surface users, and following the analysis of the lunar gravity model and the available orbits, the CON model adopting the proposed HyInc Walker configuration is detailed separately in the next section.

A. Global VOP Model of Lunar Surface

To evaluate the performance of CON for global users, the VOP model of the Moon is generated given the fact that the actual lunar surface user data is not currently available on the Moon. An alternative scheme is to deploy uniformly placed VOPs at certain latitude and longitude intervals, *i.e.*, the latitude–longitude lattice VOP (LLVOP) model, actual effect of which is shown in Fig. 2. However, this VOP deployment scheme has a major drawback, which can be clearly found in Fig. 2, the density of regional VOPs increases with increasing latitude. This may cause the subsequent algorithm to preferentially deploy operations toward larger inclinations when searching for the optimal coverage CON, bringing about a VOP latitude weighting issue that should not be introduced and further reducing the actual reference value of the CON.

Therefore, in order to avoid the phenomenon of denser points near the poles than at the equator, we no longer restrict the alternative VOP to be generated only at the intersections of discrete latitude and longitude lines, but extend it to the entire lunar sphere. To better present the uniform and stochastic distribution characteristics [51], the Fibonacci lattice [52] is introduced in this work to get the global Fibonacci lattice VOP (FLVOP) model of the lunar surface, as shown in Fig. 3.

The generation of the n^{th} point in the Fibonacci lattice is based on (consider a sphere with radius 1) :

$$z_n^1 = (2n-1)/N - 1, \tag{1a}$$

$$x_n^1 = \sqrt{1-(z_n^1)^2}\cdot\cos(2\pi n\phi), \tag{1b}$$

$$y_n^1 = \sqrt{1-(z_n^1)^2}\cdot\sin(2\pi n\phi), \tag{1c}$$

where N denotes the total number of points and the parameter ϕ is taken to obey the golden ratio under the requirement of Fibonacci lattice, *i.e.* $\phi = (\sqrt{5}-1)/2$. On this basis, multiply by the lunar radius[3] R_m to obtain the FLVOP model of the lunar surface, *i.e.* $[x_\vartheta\ y_\vartheta\ z_\vartheta] = R_m \cdot [x_n^1\ y_n^1\ z_n^1]$. $\mathbf{v}_\vartheta = [x_\vartheta\ y_\vartheta\ z_\vartheta]$ is the vector expression of VOP $\vartheta \in \mathcal{V} = \{1, 2, ..., V\}$ under MGS Coordinate System (refer to section II-C), where $\mathcal{V}$ denotes the set of points constituted by V VOPs under FLVOP model. It is observed from comparing Fig. 2 and Fig. 3 that the FLVOP model is more consistent with expectations of a uniform and stochastic distribution.

B. Lunar Gravity Model and Target Orbit

In pursuit of lower propagation time delay, Low Lunar Orbit (LLO) satellite will be the optimal choice for future lunar surface research exploration. However, compared to the Earth, the gravitational field disturbance of the Moon is more prominent and the non-spherical perturbation phenomenon[4] is more obvious due to the existence of mascons [53] below the lunar surface which is caused by the asteroid collisions. Numerous researches on lunar orbiting SATs have shown that, in order to avoid gravitational perturbations caused by mascons, the spacecraft can be deployed in LFO with orbital inclinations i of $27°, 50°, 76°, 86°$ [54], [55], where the spacecraft can maintain a long-term stable operation without crashing into the lunar surface. Alternatively, consider an orbital altitude of h_s above 750km, where the impact is already negligible [56]. Combined with the consideration that lunar SATs are exposed to more intense three-body perturbation, low altitude LFOs are prioritized in this work (yet we can set $h_s \geq 10\text{km}$ since the highest point observed by the Lunar Reconnaissance Orbiter Camera is about 10km), while the exploration of higher-orbit CON design involving three-body perturbation factors is left as an extension for future work.

As for the communication channel, combined with the fact that there are almost no gases in the lunar atmosphere, lunar SAT signal will not be severely attenuated, and the communication channel can be considered as an AWGN channel in a vacuum environment. However, the setting of the minimum communication elevation $\theta_{\min}$ also needs to take into account the existence of numerous craters on the lunar surface.

C. CON Model and HyInc Walker Configuration

1) Related Parameters of Lunar SAT Orbit: The position of a SAT is determined by six parameters, including semi-long axis a_s, eccentricity e, inclination i, longitude of RAAN Ω, perigee angle w, and the anomaly. Ω and i determine the plane of orbital motion in space, where Ω is specifically the angle between the vernal equinox and the RAAN (counterclockwise as seen from over the North Pole), and i is the angle between the orbital plane and the equatorial plane. w, a_s, and e jointly determine the specific shape of the orbit, where w is the angle between the RAAN and the perigee (direction of SAT motion), while a_s and e are the basic parameters of the ellipse with

[3]Astronomy-related parameters in this paper, including the simulation section, are referenced from the NASA official website if not specified.

[4]Consequently the deployment of lunar elliptical orbits is subject to greater perturbations than circular orbits, *e.g.* elliptical LFO (ELFO). Certainly if left out of this, LLO may not be optimum from a navigation standpoint.

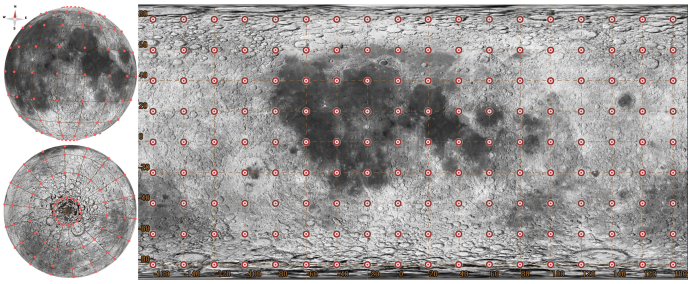

Fig. 2. LLVOP model. (Range $[80°\text{S}, 80°\text{N}]$, interval $20°$, total 162 VOPs)

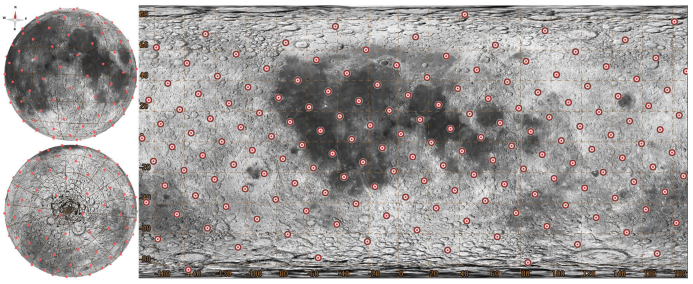

Fig. 3. FLVOP model. ($N = 162, \phi = (\sqrt{5}-1)/2 = 0.618$)

the center of the Moon as one of the focal points, and have $e, w = 0$ in a circular orbit.

The position of the SAT at a specific moment is determined by the anomaly. The anomalies are all time-varying parameters, and the departure direction of the angle is the direction of SAT motion. The true anomaly τ_A and the eccentric anomaly E_A are the angles from the perigee to the orbiting SAT and the auxiliary SAT, respectively, where the auxiliary circular orbit in which the auxiliary SAT is located has a_s as its radius and the orbital velocity is specified as the average angular velocity $\overline{w_v}$ of the orbiting SAT. Then the mean anomaly M_A at moment t can be expressed as $M_A^{(t)} = \overline{w_v} \cdot (t - t_p)$, where t_p denotes the moment at perigee, and the anomalies satisfy

$$M_A^{(t)} = E_A^{(t)} - e \cdot \sin E_A^{(t)}, \tag{2a}$$

$$\cos\tau_A^{(t)} = \frac{\cos E_A^{(t)} - e}{1 - e \cdot \cos E_A^{(t)}}. \tag{2b}$$

All the above angles range in $[0°, 360°]$, with the exception of i which takes the value $[0°, 90°]$[5].

Consider a CON of size M. In a Cartesian coordinate system with the Moon as the central celestial body, the vector $\mathbf{v}_{\mathscr{M}}^{(t)} = [x_{\mathscr{M}}^{(t)}\ y_{\mathscr{M}}^{(t)}\ z_{\mathscr{M}}^{(t)}]$ is expressed as the three-dimensional coordinates of SAT $\mathscr{M} \in \mathcal{M} = \{1, 2, ..., M\}$ at moment t, where $\mathcal{M}$ denotes the set of SAT. Concretely, the Z-axis of this coordinate system points to the lunar north pole, the X-axis points to the intersection of the first meridian plane with the equator, and the Y-axis lies on the equatorial plane and is at a $90°$ angle to the X-axis according to the right-handed coordinate system. Following the term of WGS coordinate system, this coordinate system will be called Moon Geodetic System (MGS) in this paper. Then the position of SAT $\mathscr{M}$ at moment t can be calculated by [15]

$$(\mathbf{v}_{\mathscr{M}}^{(t)})^{\mathrm{T}} = (h_s + R_m) \begin{bmatrix} \cos\Omega\cos\tau_A^{(t)} - \sin\Omega\sin\tau_A^{(t)}\cos i \\ \sin\Omega\cos\tau_A^{(t)} + \cos\Omega\sin\tau_A^{(t)}\cos i \\ \sin\tau_A^{(t)}\sin i \end{bmatrix}, \tag{3}$$

where $(\cdot)^{\mathrm{T}}$ denotes the transpose operation. And the SAT off-nadir angle β is given by the following equation:

$$\beta = \arcsin\left(\frac{R_m}{h_s + R_m} \cdot \cos\theta_{\min}\right), \tag{4}$$

the orbit radius r_s satisfies $a_s \overset{e=0}{\rightarrow} r_s = ||\mathbf{v}_{\mathscr{M}}||_2 = R_m + h_s$ in circular orbit condition, where $||\cdot||_2$ is the Euclidean norm.

[5]Due to the need for a sizable fraction of the orbiting energy to counteract the celestial rotation, retrograde orbits, *i.e.* $[90°, 180°]$, will not be considered.

Generally, orbit selection in CON construction typically considers resonant orbit, *i.e.*, the SAT rotation period T_s satisfies the following constraint:

$$\frac{T_s}{T_m} = \frac{z_1}{z_2}, z_j \in \mathbb{Z}^+, j = 1, 2, \tag{5}$$

where T_m is the rotation period of the Moon and $\mathbb{Z}^+$ denotes the set of positive integers. In the circular orbit case, combined the Kepler's 3rd Law, *i.e.*,

$$K = \frac{a_s^3}{T_s^2} = \frac{G(M_m + M_s)}{4\pi^2} \approx \frac{GM_m}{4\pi^2} \propto M_m, \tag{6}$$

where K, G, M_m, and M_s are Kepler's constant, gravitational constant, mass of Moon, and mass of SAT, respectively, h_s can then be given by

$$h_s = H_{z_2}^{z_1} \approx \sqrt[3]{\frac{GM_m}{4\pi^2} \cdot T_m^2 \cdot (\frac{z_1}{z_2})^2} - R_m, z_j \in \mathbb{Z}^+, j = 1, 2, \tag{7}$$

where $H_{z_2}^{z_1}$ denotes the resonant orbital altitude.

2) Traditional Walker: Traditional Walker is the most common of most current CON design efforts, which is relatively simple to design and deploy, manage and maintain, and has a relatively low long-term system cost. This configuration has the same height and inclination for each circular orbital plane. With a fixed h_s, the traditional Walker can be represented by a quadratic parameter set $(i/M/O/F)$, where M is the total number of SATs, O is the number of orbital planes, and F is the phase factor, which as an integer between 0 and $(O-1)$. Then by calling the first SAT in the first orbital layer the reference SAT, the longitude $\Omega^{\mathscr{M}_o}$ of the RAAN and the initial mean anomaly $M_A^{\mathscr{M}_o}$ of SAT $\mathscr{M}_o \in \mathcal{M}_o = \{1, 2, ..., M_o\}$ in orbit $o \in \mathcal{O} = \{1, 2, ..., O\}$ can be given by eq. (8) and eq. (9) as shown below:

$$\Omega^{\mathscr{M}_o} = \begin{cases} \Omega^0 + (o-1) \cdot \frac{360}{O}, i < 90°, \text{Delta}, \\ \Omega^0 + (o-1) \cdot \frac{180}{O}, i = 90°, \text{Star}, \end{cases} \tag{8}$$

$$M_A^{\mathscr{M}_o} = \left\{ \left[M_A^0 + (o-1) \cdot \Delta f\right] + (\mathscr{M}_o - 1) \cdot \frac{360}{M_o} \right\} - \left\lfloor \frac{\left\{ \left[M_A^0 + (o-1) \cdot \Delta f\right] + (\mathscr{M}_o - 1) \cdot \frac{360}{M_o} \right\}}{360} \right\rfloor \cdot 360, \tag{9}$$

where Ω^0 and M_A^0 refer to the relevant parameters of the reference SAT, M_o can indicate the number of SATs in each layer of the orbit, term $[M_A^0 + (o-1) \cdot \Delta f]$ can indicate the

initial mean anomaly of the 1st SAT in orbit o, and $\lfloor\cdot\rfloor$ is a round-down operation. The phase difference Δf is given by

$$\Delta f = \frac{360}{M} \cdot F, F \in [0, O-1], F \in \mathbb{Z}^+, \tag{10}$$

which denotes the phase relationship between the SATs of the same serial number in two adjacent orbital planes.

III. The Configuration Proposal

As mentioned earlier, the traditional Walker's trade of variety for simplicity leads to its widespread use in Earth-orbiting CON design, but also effectively excludes potential candidates for superior CON possibilities, thus making it difficult to directly apply in multi-mission requirements for LFO CON design. To address it, combining the specificity of the LFO and the generality of the configuration, we release the constraints of the traditional Walker in the inclination and develop the HyInc Walker configuration, which can also be represented by a quadratic parameter set $(\mathbf{I}/M/O/F)$, except that, unlike the traditional Walker's uniform inclination, the parameter $\mathbf{I} \in \mathbb{I}^{1\times O}$ is a vector consisting of independent i_o of each orbit, *i.e.*,

$$\mathbf{I} = [i_1 \ i_2 \ \cdots \ i_O], i_o \in \mathbb{I}, \forall o \in \mathcal{O}, \tag{11}$$

where $\mathbb{I}$ denotes the set of inclination, including all continuous values in the range $[0°, 90°]$, and can be extended to $[0°, 180°]$ under the consideration of retrograde orbit. For the LFO-based HyInc Walker, the inclination set is discrete and depends on the frozen angle, we use $\ddot{\mathbb{I}}$ to denote the frozen orbit set, and the LFO inclination set is $\ddot{\mathbb{I}}_m = \{27°, 50°, 76°, 86°\}$. Aiming to encompass the possibility of both Walker Delta and Walker Star configurations, *i.e.*, to retain the backward compatibility with the traditional Walker, the longitude $\Omega^{\mathscr{M}_o}, \forall o \in \mathcal{O}$ in HyInc Walker configuration is given by

$$\Omega^{\mathscr{M}_o} = \Omega^0 + (o-1)\cdot\frac{180}{O}\cdot\left[2 - \left(\bigvee_{o=1}^{O}\left\lfloor\frac{i_o}{90}\right\rfloor\right)\right], i_o \in [0°, 90°], \tag{12}$$

where $\bigvee$ is the disjunction symbol and the value of term $\bigvee_{o=1}^{O}\lfloor\frac{i_o}{90}\rfloor$ obeys

$$\bigvee_{o=1}^{O}\left\lfloor\frac{i_o}{90}\right\rfloor = \begin{cases} 0, \mathbf{I} \text{ without elements of } 90°, \\ 1, \mathbf{I} \text{ contains at least one } 90°, \end{cases} \tag{13}$$

and the following lemma about HyInc Walker can then be derived.

Remark 1: In this lemma and the corresponding proof, symbols that have definition conflicts with the other parts of the paper are local action symbols within the scope of this lemma and the proof. In addition, we use η, τ, δ, ξ to respectively correspond to HyInc Walker, traditional Walker, Walker Delta, and Walker Star configuration.

Lemma 1: In terms of CON performance, consider the standard MOP $\min \mathbf{\Psi}(\mathbf{X}) = [\psi_1(\mathbf{X}) \ \psi_2(\mathbf{X}) \ \cdots \ \psi_n(\mathbf{X})]$, where n is the number of objective functions ψ, $\mathbf{X} = [x_1 \ x_2 \ \cdots \ x_m]$ is the decision vector, and m is the number of decision variables. The optimal solution $\mathcal{F}_\eta^* = \{\mathbf{\Psi}_\eta^*\}$ of HyInc Walker is certainly better than or equal to $\mathcal{F}_\tau^* = \{\mathbf{\Psi}_\tau^*\}$ of traditional Walker for the same CON size M. $\mathcal{F}_\eta^*$ and $\mathcal{F}_\tau^*$ can be respectively given by eq. (44) and eq. (45) as shown in Appendix A, where $\mathbf{\Psi}^* = \mathbf{\Psi}(\mathbf{X}^*)$ and $\mathcal{F}_\delta^*, \mathcal{F}_\xi^*$ are given by eq. (46) and eq. (47).

Proof: See Appendix A. ■

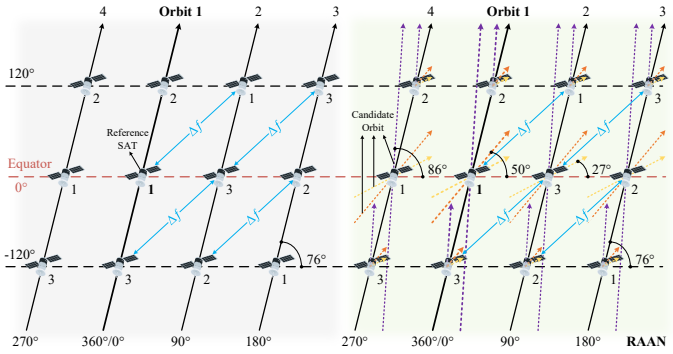

Fig. 4. Traditional Walker, $i = 76°$, (12,4,4); LFO-based HyInc Walker.

Therein, $\mathcal{P}^*$ denotes the set of pareto optimal solutions and consists of all pareto optimal points $\mathbf{X}^*$, where $\mathbf{X}^*$ is expressed as not dominated (but can be weakly dominated) by any point $\mathbf{X}$ in the decision space, *i.e.* $\nexists \mathbf{X} : \mathbf{X} \prec \mathbf{X}^*$, the symbol $\prec$ denotes domination in the standard minimization problem[6]. In addition, easily we have $\mathbf{X} \prec \mathbf{X}^* \Rightarrow \mathbf{X} \preceq \mathbf{X}^*$, where the symbol $\preceq$ denotes weak dominance, and claim that $\mathbf{X}$ and $\mathbf{X}^*$ are weakly dominated by each other under the condition that $\psi_j(\mathbf{X}^*) = \psi_j(\mathbf{X}), \forall j \in \{1, 2, ..., n\}$ is satisfied. Therefore, to state Lemma 1 in terms of decision space, $\mathcal{P}_\eta^*$ of HyInc Walker configuration is said to be definitely weakly dominating $\mathcal{P}_\tau^*$ in an overall sense[7]. And it is important to clarify that the proposed HyInc Walker configuration is a configuration-level hybrid rather than a configuration-upper level permutation hybrid, a well illustrated example of which is shown in the CON plane diagram of Fig. 4.

IV. HyInc Walker-based Lunar CNI constellation MOP formulation

In this section, we derive the relevant objective functions in the CNI constellation design, including coverage and available power in terms of communication and effective quadruple coverage and navigation positioning precision in terms of navigation. A HyInc Walker-based lunar CNI constellation MOP is then formulated.

A. Constellation Coverage Range Analysis

The coverage range indicates the performance of CON in terms of the number of services, which is numerically equivalent to the average coverage time proportion $\overline{\mathcal{C}_\mathcal{V}}$ (simply called *access coverage* in the simulation section) of all VOPs. Consider an observation of total duration T, and denote by the binary variable $\mathfrak{b}_{\vartheta,\mathscr{M}}^{(t)}$ whether the communication link between VOP ϑ and SAT $\mathscr{M}$ is available at moment $t \in \mathcal{T} = \{1, 2, ..., T\}$, where $\mathcal{T}$ denotes the set of time slots, then the following lemma about $\mathfrak{b}_{\vartheta,\mathscr{M}}^{(t)}$ can be derived.

[6]In the minimization optimization problem, we use the notation $\prec$ to denote domination [57], while in the maximization optimization problem, we use the notation $\succ$ to denote domination. This rule is followed throughout this paper.

[7]In general, the concepts of dominance and weak dominance are applied to comparisons between decision variables. The application here to comparisons between sets of decision variables is intended to show that any element in $\mathcal{P}_\tau^*$ must be weakly dominated by one or more elements in $\mathcal{P}_\eta^*$.

Lemma 2: Under circular orbit conditions, the availability of the communication link can be derived by comparing the maximum acceptable line-of-sight (LOS) component, which can be given by

$$\mathfrak{b}_{\vartheta,\mathscr{M}}^{(t)} = \begin{cases} 1, \left\| \mathbf{d}_{\vartheta,\mathscr{M}}^{(t)} \right\|_2 \leq \|\mathbf{d}_{\vartheta,\mathscr{M}}\|_2^{\max}, \\ 0, \left\| \mathbf{d}_{\vartheta,\mathscr{M}}^{(t)} \right\|_2 > \|\mathbf{d}_{\vartheta,\mathscr{M}}\|_2^{\max}, \end{cases} \tag{14}$$

where $\mathbf{d}_{\vartheta,\mathscr{M}}^{(t)} = \mathbf{v}_{\mathscr{M}}^{(t)} - \mathbf{v}_{\vartheta}^{(t)}$ denotes the vector of VOP ϑ directed to the SAT $\mathscr{M}$ at moment t in the MGS coordinate system and thus $||\mathbf{d}_{\vartheta,\mathscr{M}}^{(t)}||_2$ denotes the distance between VOP ϑ and the SAT $\mathscr{M}$. The maximum acceptable distance of the LOS component $||\mathbf{d}_{\vartheta,\mathscr{M}}||_2^{\max}$ is given by

$$||\mathbf{d}_{\vartheta,\mathscr{M}}||_2^{\max} = \sqrt{C_m^2 + h_s^2 + 2R_m h_s} - C_m, \tag{15}$$

where constant $C_m = R_m \cdot \sin(\theta_{\min})$.

Proof: See Appendix B. ■

Then the double-hop propagation delay $\Delta\tau_\vartheta$ of VOP ϑ should satisfy

$$\Delta\tau_\vartheta \leq 2\Delta\tau_{\max} = \frac{2}{c} \cdot \sqrt{C_m^2 + h_s^2 + 2R_m h_s} - C_m, \tag{16}$$

where $\Delta\tau_{\max}$ denotes the maximum single-hop time delay and c is the speed of light.

Therefore, whether the VOP ϑ is covered by CON at moment t can be obtained by

$$\mathfrak{b}_{\vartheta}^{(t)} = \bigvee_{\mathscr{M}=1}^{M} \mathfrak{b}_{\vartheta,\mathscr{M}}^{(t)}, \tag{17}$$

where $\bigvee$ is the disjunction symbol. Then the coverage time proportion $\mathcal{C}_\vartheta$ of VOP ϑ can be calculated by

$$\mathcal{C}_\vartheta = \frac{1}{T}\sum_{t=1}^{T} \mathfrak{b}_{\vartheta}^{(t)} = \frac{1}{T}\sum_{t=1}^{T} \left(\bigvee_{\mathscr{M}=1}^{M} \mathfrak{b}_{\vartheta,\mathscr{M}}^{(t)} \right), \tag{18}$$

and $\overline{\mathcal{C}_\mathcal{V}}$ can be finally obtained by

$$\overline{\mathcal{C}_\mathcal{V}} \triangleq \frac{1}{V}\sum_{\vartheta=1}^{V} \mathcal{C}_\vartheta = \frac{1}{VT}\sum_{\vartheta=1}^{V} \left[\sum_{t=1}^{T} \left(\bigvee_{\mathscr{M}=1}^{M} \mathfrak{b}_{\vartheta,\mathscr{M}}^{(t)} \right) \right]. \tag{19}$$

B. Constellation Communication Quality Analysis

Better communication quality means higher user satisfaction and is essential for time-sensitive services. For modeling the lunar SAT channel without an effective atmosphere, only the free space absorption attenuation $PL_{\mathscr{M},\vartheta}^{(t)}$ needs to be considered as follows:

$$PL_{\mathscr{M},\vartheta}^{(t)}[\mathrm{dB}] = -10\lg\left[\lambda_{\mathscr{M},\vartheta}^2 / \left((4\pi)^2 \left\| \mathbf{d}_{\mathscr{M},\vartheta}^{(t)} \right\|_2^2 \right) \right], \tag{20}$$

where the wavelength $\lambda_{\mathscr{M},\vartheta} = c/f_{\mathscr{M},\vartheta}$, $f_{\mathscr{M},\vartheta}$ is the downlink frequency. Use $G_\mathscr{M}$ and G_ϑ to denote the antenna gain[8] of SAT $\mathscr{M}$ and VOP ϑ, respectively. Then the LOS downlink signal power received at the receivers of VOP ϑ from the SAT $\mathscr{M}$ at moment t can be given by

$$\mathrm{Pr}_{\mathscr{M},\vartheta}^{(t)}[\mathrm{dBm}] = Pt_\mathscr{M}[\mathrm{dBm}] + PL_{\mathscr{M},\vartheta}^{(t)}[\mathrm{dB}] + 10\lg\left(G_\mathscr{M} G_\vartheta\right), \tag{21}$$

[8]If not obviously stated, the units used for power and gain in this paper default to the standard unit of Watt.

where $Pt_\mathscr{M}$ denotes the antenna transmission power of the SAT $\mathscr{M}$. Considering the application of inter-SAT links and SAT diversity technology, more accessible SATs means better communication tolerance performance. Then focus on the set $\mathcal{M}_\vartheta^{(t)} = \{1, 2, ..., M_\vartheta^{(t)}\}$ of available SATs above VOP ϑ at moment t, which can be calculated by

$$M_\vartheta^{(t)} = \sum_{\mathscr{M}=1}^{M} \mathfrak{b}_{\vartheta,\mathscr{M}}^{(t)}, \tag{22}$$

denoting the maximum number of available SATs, we can obtain the available power of VOP ϑ at moment t by

$$\mathrm{Pr}_\vartheta^{(t)} = \sum_{\mathscr{M}_\vartheta^{(t)}=1}^{M_\vartheta^{(t)}} \mathrm{Pr}^{(t)}\left(\mathscr{M}_\vartheta^{(t)}, \vartheta \right), \tag{23}$$

where $Pr^{(t)}(\mathscr{M}_\vartheta^{(t)}, \vartheta) = Pr_{\mathscr{M}_\vartheta^{(t)},\vartheta}^{(t)}$, which is a transformation intended for a clearer visualization of the formula. Then the time average available power of VOP ϑ can be obtained by

$$\mathcal{P}_\vartheta = \frac{1}{T}\sum_{t=1}^{T} \mathrm{Pr}_\vartheta^{(t)} = \frac{1}{T}\sum_{t=1}^{T} \left[\sum_{\mathscr{M}_\vartheta^{(t)}=1}^{M_\vartheta^{(t)}} \mathrm{Pr}^{(t)}\left(\mathscr{M}_\vartheta^{(t)}, \vartheta \right) \right], \tag{24}$$

and combined average total power $\overline{\mathcal{P}_\mathcal{V}}$ can be finally given by

$$\overline{\mathcal{P}_\mathcal{V}} \triangleq \frac{1}{V_1}\sum_{\vartheta_1=1}^{V_1} \mathcal{P}_{\vartheta_1}, \vartheta_1 \in \mathcal{V}_1 = \{\vartheta | \mathcal{P}_\vartheta > 0, \forall\vartheta \in \mathcal{V}\}, \tag{25}$$

where $\mathcal{V}_1 \subseteq \mathcal{V}, V_1 = |\mathcal{V}_1|$, and we state ϑ_1 is a registered VOP on the communication service.

C. Constellation Effective Quadruple Overlap Analysis

The basis of navigation is positioning. Considering the existence of a clock difference δt between the lunar surface receiver's clock and the on-board clock of the SAT $\mathscr{M}$, then based on the trilateration measurement principle we expect $M_\vartheta^{(t)} = \sum_{\mathscr{M}=1}^{M} \mathfrak{b}_{\vartheta,\mathscr{M}}^{(t)} \geq 4$ and can calculate the specific position of VOP ϑ by

$$\begin{cases} \sqrt{(x_1 - x_\vartheta)^2 + (y_1 - y_\vartheta)^2 + (z_1 - z_\vartheta)^2} = d_{1,\vartheta}, \\ \sqrt{(x_2 - x_\vartheta)^2 + (y_2 - y_\vartheta)^2 + (z_2 - z_\vartheta)^2} = d_{2,\vartheta}, \\ \cdots \\ \sqrt{(x_{M_\vartheta} - x_\vartheta)^2 + (y_{M_\vartheta} - y_\vartheta)^2 + (z_{M_\vartheta} - z_\vartheta)^2} = d_{M_\vartheta,\vartheta}, \end{cases} \tag{26}$$

where $d_{\mathscr{M},\vartheta} = \zeta_\mathscr{M} - \Gamma t$. $\zeta_\mathscr{M}$ denotes the pseudo-range between the SAT $\mathscr{M}$ and the receiver in the vacuum background, and $\Gamma t = c \cdot \delta t$ (*i.e.* the clock difference δt is involved in eq. (26) via the parameter d) denotes the light speed distance error term caused by the clock difference. SAT position $[x_\mathscr{M}\ y_\mathscr{M}\ z_\mathscr{M}]$ and pseudo-range $\zeta_\mathscr{M} = c \cdot (t_{\mathrm{rec}} - t_{\mathrm{tra}}^\mathscr{M})$ can be calculated via the ephemeris broadcast from each SAT, and ground segment can attribute to lunar base and inter-satellite link, where $t_{\mathrm{tra}}^\mathscr{M}$ denotes the moment when the SAT $\mathscr{M}$ transmits the signal under the on-board clock, and t_{rec} denotes the moment when the signal is received by the receiver.

TABLE I
DOP RATINGS OF LUNAR NAVIGATION CON

DOP(GPS)	Error Value	DOP	DOP^{-1}	Rating
≤ 1	$\leq 6\text{m}$	≤ 2	≥ 0.5	Ideal
$1-4$	$6-24m$	$2-8$	$0.125-0.5$	Excellent
$4-6$	$24-36m$	$8-12$	$0.083-0.125$	Good
$6-8$	$36-48m$	$12-16$	$0.063-0.083$	Moderate
$8-20$	$48-120m$	$16-40$	$0.025-0.063$	Fair
$20-50$	$120-300m$	$40-100$	$0.01-0.025$	Poor
>50	$>300m$	>100	<0.01	Useless

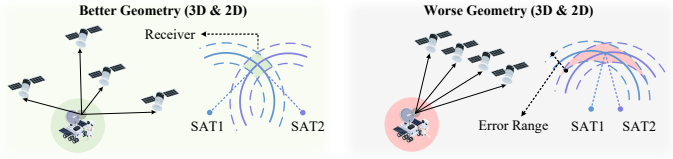

Fig. 5. Illustration of the importance of SAT geometric distribution.

Then, whether the VOP ϑ is effectively quadruple-covered by CON at moment t can be obtained by

$$\mathfrak{B}_{\vartheta}^{(t)} = \begin{cases} 0, \text{if } (\sum_{\mathscr{M}=1}^{M} \mathfrak{b}_{\vartheta,\mathscr{M}}^{(t)} < 4) \text{ or } (\mathcal{GD}_{\vartheta}^{(t)} > \mathcal{GD}^{\top}), \\ 1, \text{if } (\sum_{\mathscr{M}=1}^{M} \mathfrak{b}_{\vartheta,\mathscr{M}}^{(t)} \geq 4) \text{ and } (\mathcal{GD}_{\vartheta}^{(t)} \leq \mathcal{GD}^{\top}), \end{cases} \tag{27}$$

where $\mathcal{GD}_{\vartheta}$ denotes the GDOP [58] of VOP ϑ, representing a significant metric to describe the positioning precision in navigation, and $\mathcal{GD}^{\top}$ is an upper threshold. The optimization of geometric distribution can directly affect the performance of navigation, as shown in Fig. 5. Then the proportion of effectively quadruple-covered time of VOP ϑ can be obtained:

$$\mathcal{Q}_{\vartheta} = \frac{1}{T}\sum_{t=1}^{T} \mathfrak{B}_{\vartheta}^{(t)}, \tag{28}$$

and the average proportion $\overline{\mathcal{Q}_{\mathcal{V}}}$ (simply called *quadruple coverage* in the simulation section) can be finally given by

$$\overline{\mathcal{Q}_{\mathcal{V}}} \triangleq \frac{1}{V}\sum_{\vartheta=1}^{V} \mathcal{Q}_{\vartheta} = \frac{1}{VT}\sum_{\vartheta=1}^{V}\left(\sum_{t=1}^{T} \mathfrak{B}_{\vartheta}^{(t)}\right). \tag{29}$$

D. Constellation Dilution of Precision (DOP) Analysis

Considering the ENU coordinate system on the Moon, the positioning error $[\varepsilon_e\ \varepsilon_n\ \varepsilon_u\ \varepsilon_{\Gamma t}]$ can be calculated based on the coordinate transformation $[\varepsilon_e\ \varepsilon_n\ \varepsilon_u\ \varepsilon_{\Gamma t}]^{\mathrm{T}} = \mathbf{C^T} \cdot [\varepsilon_x\ \varepsilon_y\ \varepsilon_z\ \varepsilon_{\Gamma t}]^{\mathrm{T}}$, where $[\varepsilon_x\ \varepsilon_y\ \varepsilon_z\ \varepsilon_{\Gamma t}]^{\mathrm{T}}$ is the positioning error in MGS coordinate system and the transformation matrix is

$$\mathbf{C^T} = \begin{bmatrix} -\sin\gamma^{\mathrm{o}} & \cos\gamma^{\mathrm{o}} & 0 & 0 \\ -\sin\gamma^{\mathrm{a}}\cos\gamma^{\mathrm{o}} & -\sin\gamma^{\mathrm{a}}\sin\gamma^{\mathrm{o}} & \cos\gamma^{\mathrm{a}} & 0 \\ \cos\gamma^{\mathrm{a}}\cos\gamma^{\mathrm{o}} & \cos\gamma^{\mathrm{a}}\sin\gamma^{\mathrm{o}} & \sin\gamma^{\mathrm{a}} & 0 \\ 0 & 0 & 0 & 1 \end{bmatrix}, \tag{30}$$

where γ^o and γ^a are the receiver's longitude and latitude. The relationship between $[\varepsilon_e\ \varepsilon_n\ \varepsilon_u\ \varepsilon_{\Gamma t}]$ and the measurement error ε_ρ is given by [59]:

$$[\varepsilon_e\ \varepsilon_n\ \varepsilon_u\ \varepsilon_{\Gamma t}]^{\mathrm{T}} = (\mathbf{G}^{\mathrm{T}}\mathbf{G})^{-1}\mathbf{G}^{\mathrm{T}}\boldsymbol{\varepsilon}_{\rho}, \tag{31}$$

and $\mathbf{G}$ is the geometric matrix, $-\mathbf{G}_{\vartheta}$ equals to

$$\begin{bmatrix} \cos\theta_1\sin\alpha_1 & \cos\theta_1\cos\alpha_1 & \sin\theta_1 & -1 \\ \cos\theta_2\sin\alpha_2 & \cos\theta_2\cos\alpha_2 & \sin\theta_2 & -1 \\ \cdots & \cdots & \cdots & \cdots \\ \cos\theta_{M_\vartheta}\sin\alpha_{M_\vartheta} & \cos\theta_{M_\vartheta}\cos\alpha_{M_\vartheta} & \sin\theta_{M_\vartheta} & -1 \end{bmatrix}, \tag{32}$$

where θ and α denote elevation and azimuth angle respectively. $\boldsymbol{\varepsilon}_\rho = [-\varepsilon_{1,\rho} - \varepsilon_{2,\rho} \cdots - \varepsilon_{M,\rho}]^{\mathrm{T}}$ reflects the total error excluding the clock difference. Based on the background of the lunar CON, we can model its measurement error with the following two assumptions [60], which are justified and useful for the simplification and derivation of the positioning error covariance matrix.

Assumption 1: Lunar SAT's measurement error obey a normal distribution with $\mathbb{E}(\varepsilon_\rho) = 0$[9], $\mathbb{V}(\varepsilon_\rho) = \sigma^2$, where $\mathbb{E}(\cdot)$ and $\mathbb{V}(\cdot)$ denote expectation and variance operator, respectively.

Assumption 2: Measurement errors between lunar SATs are uncorrelated. The ionospheric model in GPS may cause errors to be highly correlated, whereas it's reasonable on the Moon.

Remark 2: Since no atmospheric influence and basically no multipath phenomenon exists due to the buildings or other factors, we only need to consider the standard deviation related to the control section σ_{CS} (3m in GPS), *i.e.* $\sigma_{\mathrm{CS}}^2 = \sigma^2$ ($5.916\text{m} \approx 6\text{m}$ in GPS). The DOP ratings of lunar navigation CON referenced from GPS [61] are shown in Table I.

Lemma 3: Lunar VOP's positioning error covariance matrix $\mathbf{Diag}^{-}(\sigma_e^2, \sigma_n^2, \sigma_u^2, \sigma_{\Gamma t}^2) = \sigma^2\mathbf{W}$, where $\mathbf{Diag}^{-}(\cdot)$ denotes a non-necessarily imposed diagonal matrix, $\sigma_e^2, \sigma_n^2, \sigma_u^2, \sigma_{\Gamma t}^2$ is each positioning error component's variance and $\mathbf{W} = \mathbf{Diag}^{-}(w_{11}, w_{22}, w_{33}, w_{44}) = (\mathbf{G}^{\mathrm{T}}\mathbf{G})^{-1}$ is the weight coefficient matrix.

Proof: See Appendix C. ■

Then the GDOP of VOP ϑ at moment t can be given by

$$\mathcal{GD}_{\vartheta}^{(t)} = \sqrt{w_{11}^{(t)} + w_{22}^{(t)} + w_{33}^{(t)} + w_{44}^{(t)}} = \sqrt{\mathrm{Tr}(\mathbf{W}_{\vartheta}^{(t)})}, \tag{33}$$

and the time average value $\mathcal{GD}_{\vartheta}$ can be calculated by

$$\mathcal{GD}_{\vartheta} = \frac{1}{T}\sum_{t=1}^{T}\left[\sqrt{\mathrm{Tr}(\mathbf{W}_{\vartheta}^{(t)})}\right], \tag{34}$$

thus combined average GDOP $\overline{\mathcal{GD}_{\mathcal{V}}}$[10] can be obtained by

$$\overline{\mathcal{GD}_{\mathcal{V}}} \triangleq \frac{1}{V_2}\sum_{\vartheta_2=1}^{V_2} \mathcal{GD}_{\vartheta_2}, \vartheta_2 \in \mathcal{V}_2 = \{\vartheta | \exists \mathfrak{B}_{\vartheta}^{(t)} = 1, \forall \vartheta \in \mathcal{V}\}, \tag{35}$$

where $\mathcal{V}_2 \subseteq \mathcal{V}, V_2 = |\mathcal{V}_2|$, and we state ϑ_2 is a registered VOP on the navigation service.

E. Problem Formulation

Based on the above analysis and considering the joint optimization of communication performance and navigation

[9]For system-level analysis with accuracy several orders of magnitude lower (*e.g.* meters/decimeters), this is reasonable. Certainly for precise orbit determination (*e.g.* at few centimeters level), non-zero mean considerations are more realistic and important for research with small systematic errors.

[10]In the simulation section, the description "combined average geometric precision" is relevant. In conclusion, this metric provides an overall reflection of the CON network's performance in terms of navigation service quality.

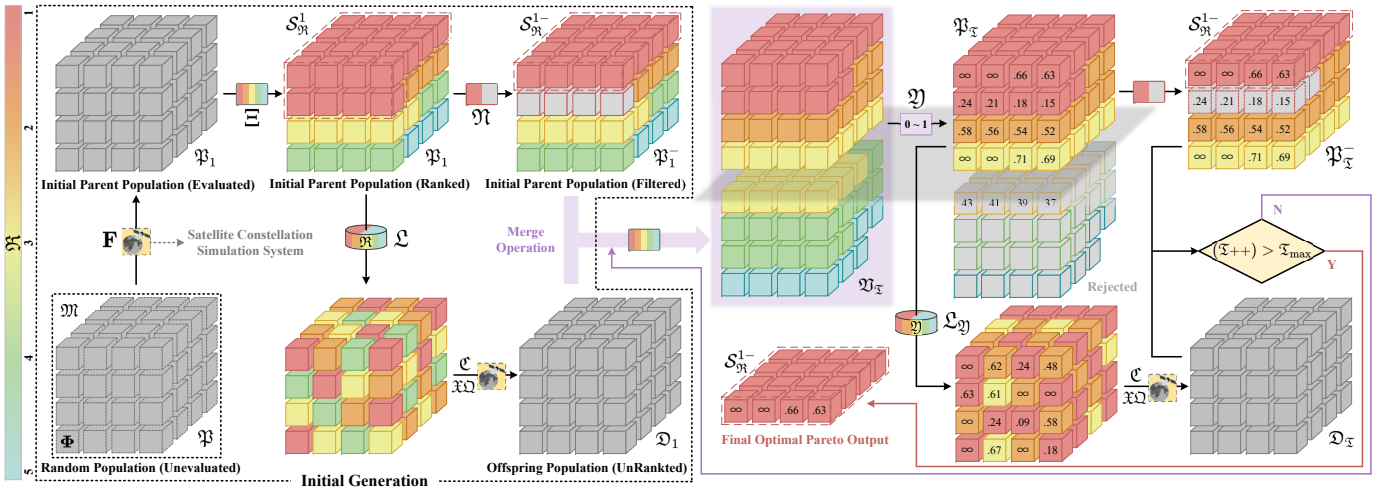

Fig. 6. A detailed flow illustration of the whole solution. (Assuming the pareto front maximum level is 5)

performance, the MOP (P0) for HyInc Walker-based lunar CNI constellation is formulated as follows:

$$(\text{P0}): \max_{h_s,\mathbf{I},M,O,F,\Omega^0,M_A^0} \left(\overline{\mathcal{C}_\mathcal{V}}, \overline{\mathcal{P}_\mathcal{V}}, \overline{\mathcal{Q}_\mathcal{V}}, -\overline{\mathcal{GD}_\mathcal{V}}\right), \tag{36a}$$

$$\text{s.t.} \quad 10 \le h_s \le 750, h_s = H_{z_2}^{z_1}, z_1, z_2 \in \mathbb{Z}^+, \tag{36b}$$

$$0^\circ \le i_o \le 90^\circ, i_o \in \mathbf{I} = [i_1 \ i_2 \ \cdots \ i_O], \tag{36c}$$

$$M_o = M/O \in \mathbb{Z}^+, \tag{36d}$$

$$F \in \{0, 1, ..., O-1\}, \tag{36e}$$

$$0^\circ \le \Omega^0, M_A^0 \le 360^\circ, \tag{36f}$$

$$\Omega^{\mathscr{M}_o} \text{ obeys eq. (12)}, M_A^{\mathscr{M}_o} \text{ obeys eq. (9)}, \tag{36g}$$

and it should be noted that given the experimental complexity, eq. (36b) will be eliminated from the simulation research of this work, *i.e.*, h_s will be directly given as some $H_{z_2}^{z_1}$, since this is not the focus of this work.

V. Solution and Algorithms

In this section, we first start with the modeling of two sub-MOPs and discuss the simplification of (P0) based on their analysis. Then, we present the pareto fraction-involved non-dominated sorting genetic algorithm-II (NSGA-II) and its application process in combination with CON simulation system in this lunar CNI CON design.

A. Modeling of Sub-MOPs and Simplification of (P0)

Before solving (P0), setting $\mathbf{\Phi}$ to denote CON parameters, *i.e.* $\mathbf{\Phi} = [h_s \ \mathbf{I} \ M \ O \ F \ \Omega^0 \ M_A^0]$, we consider two sub-MOPs:

$$(\text{P1}): \max_{\mathbf{\Phi}} \ \overline{\mathcal{C}_\mathcal{V}}, \overline{\mathcal{P}_\mathcal{V}}, \quad \text{s.t. eq. (36b)-(36g)}, \tag{37}$$

$$(\text{P2}): \max_{\mathbf{\Phi}} \ \overline{\mathcal{Q}_\mathcal{V}}, -\overline{\mathcal{GD}_\mathcal{V}}, \quad \text{s.t. eq. (36b)-(36g)}, \tag{38}$$

where (P1) is the HyInc Walker-based lunar communication CON MOP and (P2) is the HyInc Walker-based lunar navigation CON MOP. The significance of this approach includes, on the one hand, a more comprehensive analysis and available conclusions for each objective in terms of communication and navigation, including the validation of the performance improvement by applying the proposed configuration, and on the other hand, a simplification of (P0) by using a "product-ratio model" for the specificity of MOP in this paper, based on a theoretical comparison of the solution phenomenon with the linear weighted model tradeoff.

Specifically, we consider the product $(\overline{\mathcal{C}_\mathcal{V}} \cdot \overline{\mathcal{P}_\mathcal{V}})$ and the ratio $(\overline{\mathcal{Q}_\mathcal{V}}/\overline{\mathcal{GD}_\mathcal{V}})$ as a combined measurement of CON's *communication performance* and *navigation performance*, respectively. Compared to linear weighted model, it avoids the problem of comparing and combining magnitudes. And considering DOP^{-1} (as shown in Table I) as an accuracy factor as well, we can easily know that both $(\overline{\mathcal{C}_\mathcal{V}} \cdot \overline{\mathcal{P}_\mathcal{V}})$ and $(\overline{\mathcal{Q}_\mathcal{V}}/\overline{\mathcal{GD}_\mathcal{V}})$ contain significant physical meanings. Therefore, MOP (P1) can be simplified to (P3) as shown below:

$$(\text{P3}): \max_{\mathbf{\Phi}} \ \overline{\mathcal{C}_\mathcal{V}} \cdot \overline{\mathcal{P}_\mathcal{V}}, \overline{\mathcal{Q}_\mathcal{V}}/\overline{\mathcal{GD}_\mathcal{V}}, \quad \text{s.t. eq. (36b)-(36g)}. \tag{39}$$

B. Pareto Fraction-involved NSGA-II for CON Design

As mentioned earlier, in order to enhance the applicability and reference significance of the integrated CON designed for the Moon, the construction of the CON simulation system, the pareto model [62], [63] and the application of NSGA-II [57] are all considered for the solution of (P1), (P2) and (P3), where NSGA-II has been a widely popular and efficient multi-objective genetic algorithm [30]. Then each $\mathbf{\Phi}$ becomes a genetic individual, and $h_s, \mathbf{I} = [i_1 \ i_2 \ \cdots \ i_O], M, O, F, \Omega^0, M_A^0$ is individual trait. To better accommodate the CON diversity during the selection operation, additionally, we consider pareto fraction-involved[11] NSGA-II and integrate the representation:

$$\text{NSGA-II} = (\mathfrak{M}, \mathfrak{P}, \mathfrak{D}, \mathbf{F}, \Xi, \mathfrak{N}, \mathfrak{Y}, \mathfrak{L}_\mathfrak{Y}, \mathfrak{C}, \mathfrak{X}, \mathfrak{Q}, \mathfrak{T}), \tag{40}$$

where $\mathfrak{M}$ is the CON population size, $\mathfrak{P}, \mathfrak{D}$ respectively denote the parent and offspring CON population, $\mathbf{F}$ is the CON evaluation function vector, Ξ denotes the CON fast non-dominated sorting process, $\mathfrak{N}$ is the pareto fraction, $\mathfrak{Y}$ denotes the crowded comparison process, $\mathfrak{L}_\mathfrak{Y}$ denotes the binary tournament selection operator[12] based on crowded comparison,

[11] Original NSGA-II achieves elite maintenance by complete merging of parent-offspring, however, this may tend to fall into a highly correlated local optimum with the parent prematurely. While pareto fraction limits the number of individuals involved in merging at the parent-optimal nondominant level.

[12] The binary tournament selection operator randomly selects two individuals (put-back sampling) and compares the fitness values (*i.e.* rank) for merit retention, and keeps cycling until the number of retention reaches the population size $\mathfrak{M}$.

Algorithm 1: Constellation Fast Nondominated Sort Ξ

Input: All constellation individual $\mathbf{\Phi} \in \mathcal{S}_{\mathbf{\Phi}}$, $\mathbf{\Phi} = [h_s\ \mathbf{I}\ M\ O\ F\ \Omega^0\ M_A^0]$, $\mathbf{F}$.

1 **Initialization**: Pareto front counter $l = 1$;
2 **for** *each constellation individual* $\mathbf{\Phi} \in \mathcal{S}_{\mathbf{\Phi}}$ **do**
3 $\mathcal{D}^{\mathbf{\Phi}} = \emptyset$, $|\mathcal{D}_{\mathbf{\Phi}}| = 0$;
4 **for** *other constellation individual* $\mathbf{\Theta} \in \mathcal{S}_{\mathbf{\Phi}}$ **do**
5 **if** $\mathbf{\Phi} \succ \mathbf{\Theta}(\leftarrow \mathbf{F})$ **then**
6 $\mathcal{D}^{\mathbf{\Phi}} = \mathcal{D}^{\mathbf{\Phi}} \cup \{\mathbf{\Theta}\}$;
7 **else if** $\mathbf{\Theta} \succ \mathbf{\Phi}(\leftarrow \mathbf{F})$ **then**
8 $|\mathcal{D}_{\mathbf{\Phi}}| = |\mathcal{D}_{\mathbf{\Phi}}| + 1$;
9 **if** $|\mathcal{D}_{\mathbf{\Phi}}| = 0$ **then**
10 $\mathfrak{R}(\mathbf{\Phi}) = 1$, $\mathcal{S}_{\mathfrak{R}}^1 = \mathcal{S}_{\mathfrak{R}}^1 \cup \{\mathbf{\Phi}\}$;
11 **while** l^{th} *pareto front* $\mathcal{S}_{\mathfrak{R}}^l \neq \emptyset$ **do**
12 Temporary set $\mathcal{S}_{\text{temp}} = \emptyset$ for next pareto front;
13 **for** *each constellation individual* $\mathbf{\Phi} \in \mathcal{S}_{\mathfrak{R}}^l$ **do**
14 **for** *each constellation individual* $\mathbf{\Theta} \in \mathcal{D}^{\mathbf{\Phi}}$ **do**
15 $|\mathcal{D}_{\mathbf{\Theta}}| = |\mathcal{D}_{\mathbf{\Theta}}| - 1$;
16 **if** $|\mathcal{D}_{\mathbf{\Theta}}| = 0$ **then**
17 $\mathfrak{R}(\mathbf{\Theta}) = l + 1$, $\mathcal{S}_{\text{temp}} = \mathcal{S}_{\text{temp}} \cup \{\mathbf{\Theta}\}$;
18 $l = l + 1$, $\mathcal{S}_{\mathfrak{R}}^l = \mathcal{S}_{\text{temp}}$;

Output: $\mathcal{D}^{\mathbf{\Phi}}, |\mathcal{D}_{\mathbf{\Phi}}|, \forall \mathbf{\Phi} \in \mathcal{S}_{\mathbf{\Phi}}, \mathcal{S}_{\mathfrak{R}}^l, \forall l$.

$\mathfrak{C}$ is the genetic codeword rule, $\mathfrak{X}, \mathfrak{Q}$ are the recombination and variation operators, $\mathfrak{T}$ denotes the termination condition of a genetic operation. One termination condition is to let $\mathfrak{T}$ denote the current generation and let $\mathfrak{T}_{\max}$ decide when to terminate.

1) Evaluation Function $\mathbf{F}$ *and CON Simulation System:* For the maximization problem, CON evaluation function $\mathbf{F} = [\mathfrak{F}_1\ \mathfrak{F}_2]$ can be obtained directly by converting the objective function $f^{\text{obj}}(\mathbf{\Phi})$, as shown in eq. (42), where C_{low}^+ is a suitably small positive integer and the value of the objective function $f^{\text{obj}}(\mathbf{\Phi})$ is demanded to be obtained by the CON simulation system.

2) CON Fast Nondominated Sorting Approach Ξ*:* Combined with footnote 6, in (P1), (P2) and (P3) we state that CON $\mathbf{\Phi}_1$ dominates $\mathbf{\Phi}_2$, *i.e.* $\mathbf{\Phi}_1 \succ \mathbf{\Phi}_2$, when both $\mathfrak{F}_1(\mathbf{\Phi}_1) > \mathfrak{F}_1(\mathbf{\Phi}_2)$ and $\mathfrak{F}_2(\mathbf{\Phi}_1) > \mathfrak{F}_2(\mathbf{\Phi}_2)$ hold. Then the fitness (or rank) $\mathfrak{R}(\mathbf{\Phi})$ of $\mathbf{\Phi}$ which is equal to its nondomination level can be obtained through Algorithm 1, where $\mathcal{S}_{\mathbf{\Phi}}$ is the set of all CONs, $\mathcal{D}^{\mathbf{\Phi}}$ and $\mathcal{D}_{\mathbf{\Phi}}$ denote the sets constituted by the CONs dominated by, and dominating CON $\mathbf{\Phi}$ in $\mathcal{S}_{\mathbf{\Phi}}$, respectively, while $\mathcal{S}_{\mathfrak{R}}^l$ is the set of CON individuals corresponding to the l^{th} level of the pareto front. "$(\leftarrow \mathbf{F})$" in line 5 and line 7 of the algorithm indicates that the process requires the cooperation of the CON simulation system.

3) Pareto Fraction $\mathfrak{N}$*-involved Elitist-Preserving Approach:* The actual individuals that get to participate in the merge in the optimal pareto set of the parent will be limited to $(\mathfrak{N} \cdot \mathfrak{M})$.

4) Crowded Comparison $\mathfrak{Y}$*-based Binary Tournament Selection Operator* $\mathfrak{L}_{\mathfrak{Y}}$*:* The crowding distance $\mathfrak{S}(\mathbf{\Phi}^l)$ of CON $\mathbf{\Phi}^l \in \mathcal{S}_{\mathfrak{R}}^l$ of the l^{th} layer pareto front is given by eq. (43). $\mathfrak{S}(\mathbf{\Phi})$ can describe the density of solutions around CON $\mathbf{\Phi}$ in pareto function space, and its larger size means lower density and the front tends to be uniformly dispersed, which is conducive to diversity preservation. n^{obj} in eq. (43) refers to the number of objective functions, $\mathbf{\Phi}_{\text{left}}^l, \mathbf{\Phi}_{\text{right}}^l$ denote the nearest left and right neighbors in the l^{th} layer pareto front to CON $\mathbf{\Phi}^l$, respectively. Then based on eq. (43), the crowded comparison operator $\succ_{\mathfrak{Y}}$ can be defined:

$$\begin{aligned} &\mathbf{\Phi}_1 \succ_{\mathfrak{Y}} \mathbf{\Phi}_2, \text{ if } \mathfrak{R}(\mathbf{\Phi}_1) < \mathfrak{R}(\mathbf{\Phi}_2) \text{ or} \\ &\mathfrak{R}(\mathbf{\Phi}_1) = \mathfrak{R}(\mathbf{\Phi}_2)\ \&\ \mathfrak{S}(\mathbf{\Phi}_1) > \mathfrak{S}(\mathbf{\Phi}_2), \end{aligned} \tag{41}$$

belonging to a parameterless niching operator (partial order). And $\mathfrak{L}_{\mathfrak{Y}}$ is the binary tournament selection based on $\succ_{\mathfrak{Y}}$.

Genetic code rule $\mathfrak{C}$, recombination operator $\mathfrak{X}$ and mutation operator $\mathfrak{Q}$ are the same as in the traditional genetic algorithm (GA). Fig. 6 is a detailed flow illustration of the whole solution and the pseudo code of main loop is shown in Algorithm 2, where the set marked with a minus sign denotes the remaining set after the relevant elements are eliminated.

Algorithm 2: $\mathfrak{N}$-involved NSGA-II (Main Loop)

Input: $\mathbf{F}$, $\mathfrak{M}$, $\mathfrak{N}$-processed initial parent constellation population $\mathfrak{P}_1^-$, first offspring population $\mathfrak{D}_1$.

Initialization: Current generation $\mathfrak{T} = 2$;
while *current generation* $\mathfrak{T} \leq \mathfrak{T}_{\max}$ **do**
 $\mathfrak{V}_{\mathfrak{T}} = \mathfrak{P}_{\mathfrak{T}-1}^- \cup \mathfrak{D}_{\mathfrak{T}-1}$, $\mathcal{S}_{\mathfrak{R}}^l = \Xi(\mathfrak{V}_{\mathfrak{T}}), \forall l$;
 $\mathfrak{P}_{\mathfrak{T}} = \emptyset$, $l = 1$;
 while $|\mathfrak{P}_{\mathfrak{T}}| + |\mathcal{S}_{\mathfrak{R}}^l| \leq \mathfrak{M}$ **do**
 Calculate $\mathfrak{S}(\mathbf{\Phi}^l), \forall \mathbf{\Phi}^l \in \mathcal{S}_{\mathfrak{R}}^l$ based on eq. (43);
 $\text{Sort}(\mathcal{S}_{\mathfrak{R}}^l, \succ_{\mathfrak{Y}})$, $\mathfrak{P}_{\mathfrak{T}} = \mathfrak{P}_{\mathfrak{T}} \cup \mathcal{S}_{\mathfrak{R}}^l$, $l = l + 1$;
 $\text{Sort}(\mathcal{S}_{\mathfrak{R}}^l, \succ_{\mathfrak{Y}})$, $\mathfrak{P}_{\mathfrak{T}} = \mathfrak{P}_{\mathfrak{T}} \cup \mathcal{S}_{\mathfrak{R}}^l[1 : (\mathfrak{M} - |\mathfrak{P}_{\mathfrak{T}}|)]$;
 $\mathcal{S}_{\mathfrak{R}}^{1-} = \mathcal{S}_{\mathfrak{R}}^1[1 : (\mathfrak{M} \cdot \mathfrak{N})]$, $\mathfrak{P}_{\mathfrak{T}}^- = \mathfrak{P}_{\mathfrak{T}} - (\mathcal{S}_{\mathfrak{R}}^1 - \mathcal{S}_{\mathfrak{R}}^{1-})$;
 $\mathfrak{P}_{\mathfrak{T}} \xrightarrow{\mathfrak{L}_{\mathfrak{Y}}, \mathfrak{C}, \mathfrak{X}, \mathfrak{Q}, \mathbf{F}} \mathfrak{D}_{\mathfrak{T}}$, $\mathfrak{T} = \mathfrak{T} + 1$;

Output: $\mathcal{S}_{\mathfrak{R}}^{1-}$ in generation $\mathfrak{T}_{\max}$.

TABLE II
MAIN PARAMETERS FOR SIMULATION

Parameter	Value
Gravity model, Gravitational paramter (km^3/s^2)	GL0660B, 4902.8
Lunar radius R_m (km), Orbital altitude h_s (km)	1737.40, 500
Propagator, Duration (day), Time step (sec)	TwoBody,27.32,60
Minimum elevation angle $\theta_{\min}$	15°
Transmission power $Pt_{\mathscr{M}}$ (W)	10
Antenna gain $G_{\mathscr{M}}, G_{\vartheta}$ (dB)	30, 30
Downlink frequency $f_{\mathscr{M},\vartheta}$ (GHz)	30
Precision upper threshold $\mathcal{GD}^{\top}$	100
Population size $\mathfrak{M}$, Pareto fraction $\mathfrak{N}$	50, 0.3
Maximum generation $\mathfrak{T}_{\max}$	100
Reference satellite parameters Ω^0, M_A^0	0°, 0°

VI. SIMULATION RESULT

In this section, we conduct a series of simulations considering the FLVOP model and the CON model presented in section II and section III, and the detailed results are then presented and fully analyzed, including the performance of the proposed configuration. The main parameters, including the algorithm parameters [27] and the antenna parameters with reference to the existing LEO CON [64], are listed in Table II, where some other parameters of the reference SAT are reasonable settings owing to the global FLVOP model and $h_s = H_{248}^1 \rightarrow \Delta_{\tau_{\max}} < 5\text{ms}$.

$$[\mathbf{F}(\mathbf{\Phi})]^{\mathrm{T}} = \begin{bmatrix} \mathfrak{F}_1(\mathbf{\Phi}) \\ \mathfrak{F}_2(\mathbf{\Phi}) \end{bmatrix} = \begin{bmatrix} f_1^{\mathrm{obj}}(\mathbf{\Phi}) + C_{\mathrm{low}}^{+}, \text{if } f_1^{\mathrm{obj}}(\mathbf{\Phi}) + C_{\mathrm{low}}^{+} > 0;\ 0, \text{if } f_1^{\mathrm{obj}}(\mathbf{\Phi}) + C_{\mathrm{low}}^{+} \le 0 \\ f_2^{\mathrm{obj}}(\mathbf{\Phi}) + C_{\mathrm{low}}^{+}, \text{if } f_2^{\mathrm{obj}}(\mathbf{\Phi}) + C_{\mathrm{low}}^{+} > 0;\ 0, \text{if } f_2^{\mathrm{obj}}(\mathbf{\Phi}) + C_{\mathrm{low}}^{+} \le 0 \end{bmatrix}. \tag{42}$$

$$\mathfrak{S}(\mathbf{\Phi}^l) = \infty \text{ if } \mathbf{\Phi}^l \in \left\{ \arg\max_{\mathbf{\Phi}^l} f_1^{\mathrm{obj}}(\mathbf{\Phi}^l), \arg\min_{\mathbf{\Phi}^l} f_1^{\mathrm{obj}}(\mathbf{\Phi}^l) \right\} \text{else}$$
$$\sum_{j=1}^{n^{\mathrm{obj}}} \frac{f_j^{\mathrm{obj}}(\mathbf{\Phi}^l_{\mathrm{right}}) - f_j^{\mathrm{obj}}(\mathbf{\Phi}^l_{\mathrm{left}})}{\max\left\{ f_j^{\mathrm{obj}}(\mathbf{\Phi}^l) | \mathbf{\Phi}^l \in \mathcal{S}^l_{\mathfrak{R}} \right\} - \min\left\{ f_j^{\mathrm{obj}}(\mathbf{\Phi}^l) | \mathbf{\Phi}^l \in \mathcal{S}^l_{\mathfrak{R}} \right\}}. \tag{43}$$

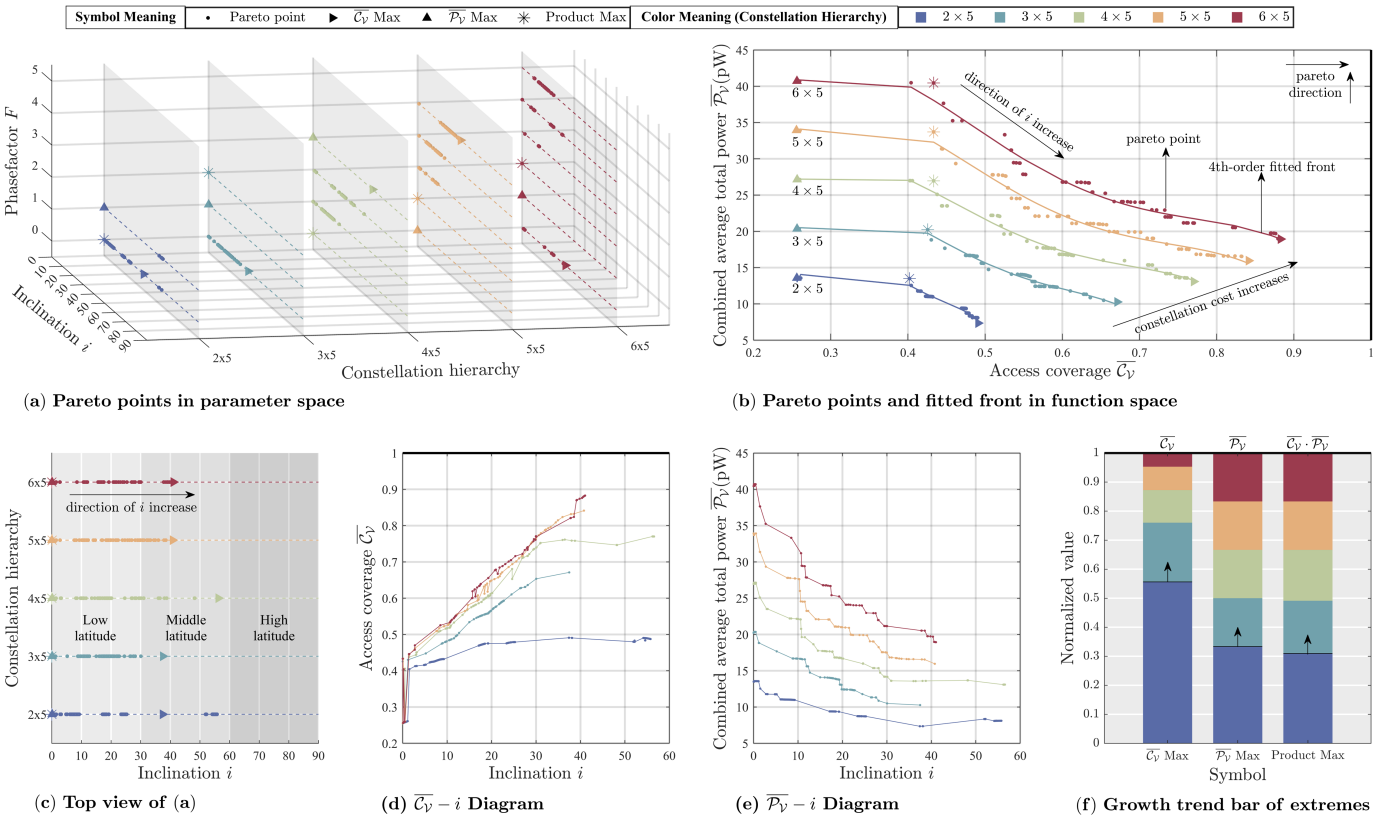

(a) Pareto points in parameter space

(b) Pareto points and fitted front in function space

(c) Top view of (a)

(d) $\overline{\mathcal{C}_\mathcal{V}} - i$ Diagram

(e) $\overline{\mathcal{P}_\mathcal{V}} - i$ Diagram

(f) Growth trend bar of extremes

Fig. 7. The pareto space behavior of MOP (P1) under traditional Walker. ("2 × 5" means two orbits with 5 SATs per orbit, same elsewhere)

A. *Pareto Space Analysis under traditional Walekr CON*

Fig. 7 and Fig. 8 show the pareto space comprehensive situation of MOP (P1) and (P2) under Walker CON model, respectively. Jointly Fig. 7(b) and Fig. 8(a), a clear and realistic conclusion is that an increase in CON size always enhances the performance of CON in various aspects. For communication CONs, by combining the parameter space and function space shown in Fig. 7(a) and Fig. 7(b), several conclusions can be summarized. *First*, at fixed scale cost, access coverage can be improved by increasing i, where F aids in selecting specific CONs that cover as few overlapping areas as possible in CON operation, but this comes at the cost of user average total power. And from Fig. 7(c), it can be noticed that the zero-inclination CONs have the best average total power performance, benefiting from the fact that they serve fewer users due to more serious coverage overlaps. *Second*, it can also be noticed from Fig. 7(c) that CONs with high latitude inclinations are all poor solutions. This suggests that the continued increase in i leads to more overlapping regions, reducing the utilization of the CONs in terms of coverage resources (embodied in the missing second half of the line segment in Fig. 7(d), yet without trading off a satisfactory enhancement in the quality of communication. It

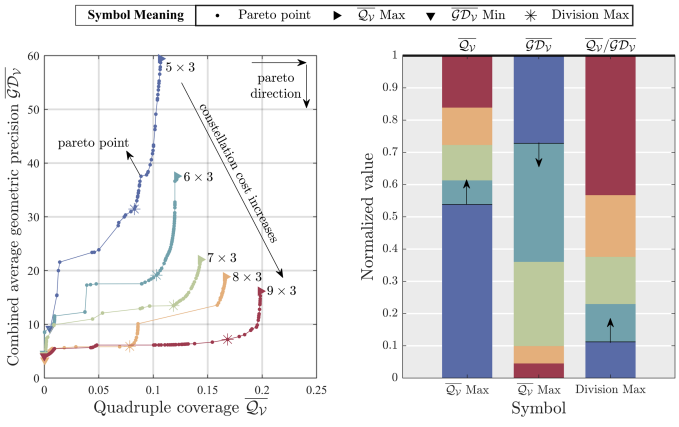

(a) Pareto points in function space

(b) Growth trend bar of extremes

Fig. 8. The pareto space behavior of MOP (P2) under traditional Walker.

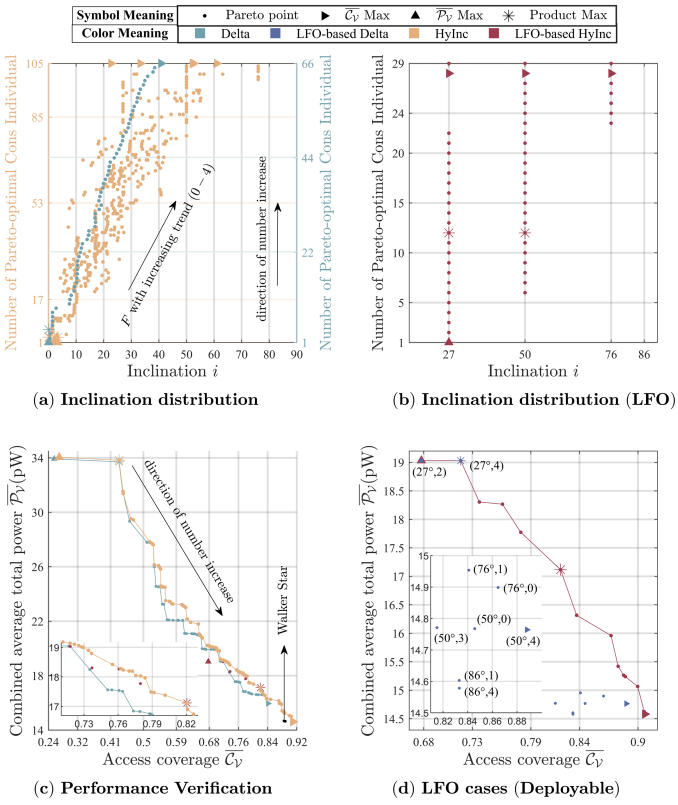

(a) **Inclination distribution** (b) **Inclination distribution (LFO)**

(c) **Performance Verification** (d) **LFO cases (Deployable)**

Fig. 9. Configuration comparison in (P1). (Hierarchy: 5×5)

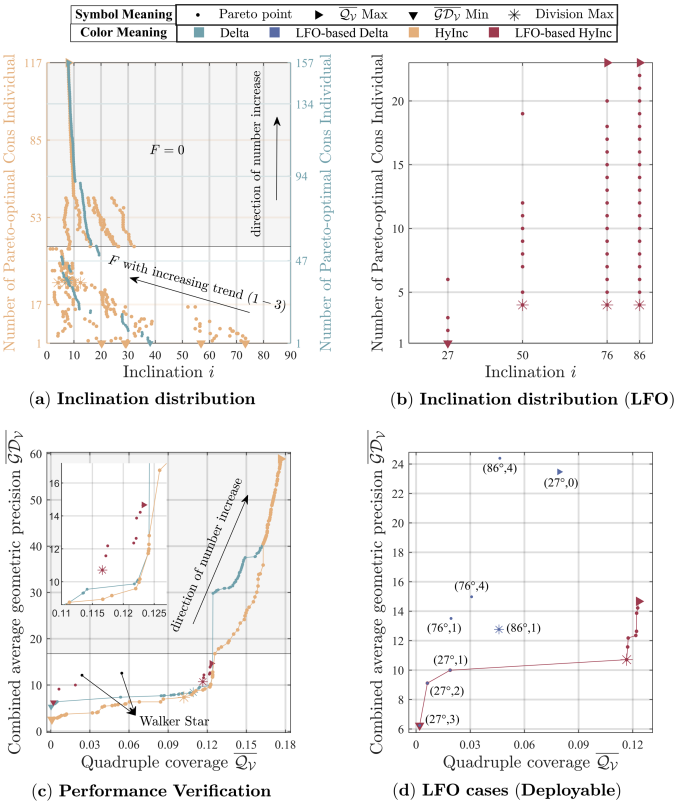

(a) **Inclination distribution** (b) **Inclination distribution (LFO)**

(c) **Performance Verification** (d) **LFO cases (Deployable)**

Fig. 10. Configuration comparison in (P2). (Hierarchy: 5×5)

can be deduced that the improvement in average total power that can be obtained by further increasing i has slowed down, which is exactly consistent with Fig. 7(e). *Third*, despite the degradation of average total power, a guiding conclusion can be drawn by combining Fig. 7(b) and Fig. 7(c), *i.e.*, for CONs pursuing optimal average total power, slightly compromising the average total power of individual users earns an access coverage improvement of nearly 20%. Exhibiting this in the physical space, a slight increase in i can cover more users with almost no degradation of the average total power, which allows for a better utilization of the CON resources.

As for the navigation CONs, it can be seen from Fig. 8(a) that a slight cut in the number of services for navigation CONs pursuing the number of services can bring up to 50% improvement in GDOP to the remaining users. In addition, comparing Fig. 7(b) and Fig. 8(a), as expected, due to the higher cost of scale required for low orbit CONs for quadruple coverage, the size of a navigation CON needs to be multifold compared with that of a communication CON in order to achieve the same number of services, which can also be analyzed from the growth trend of the first left-hand column of bar in Fig. 7(f) and Fig. 8(b).

Fig. 7(f) and Fig. 8(b) enable to analysis of the relationship between each performance metric and CON size in SOPs. For communication CONs pursuing optimal access coverage, CON size requirement is not large, and the coverage enhancement brought about by the growth in size is no longer significant afterward. For communication CONs that optimize quality or overall communication performance, the performance metrics are almost linearly related to CON size. For navigation CONs aiming for the optimal number of coverage, CON size

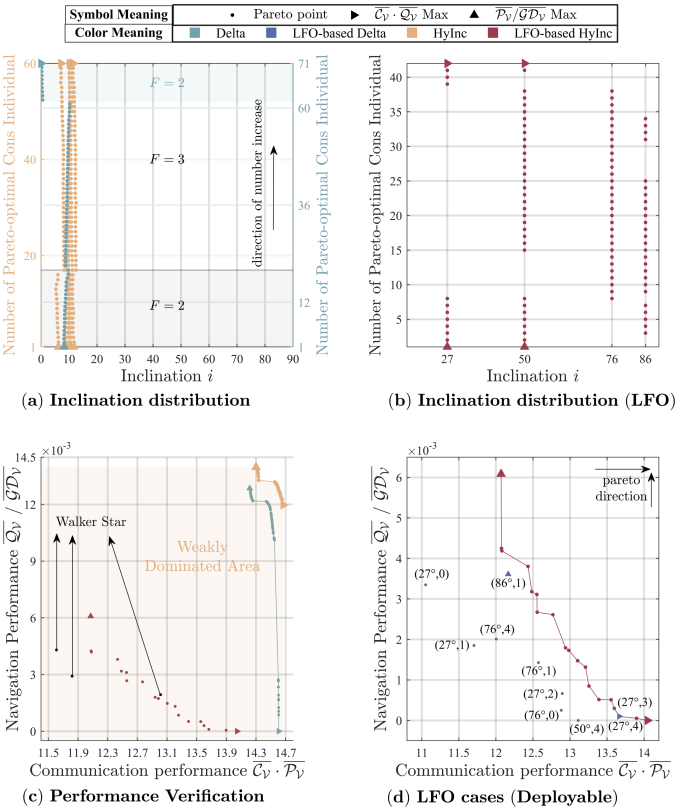

(a) **Inclination distribution** (b) **Inclination distribution (LFO)**

(c) **Performance Verification** (d) **LFO cases (Deployable)**

Fig. 11. Configuration comparison in (P3). (Hierarchy: 5×5)

requirements are much larger due to the challenges of low orbital altitude and quadruple coverage. It can be found that during the growth from "5×3" to "9×3", the decrease of

TABLE III
LFO-BASED HYINC WALKER PARAMETERS OF PARETO CON ((P1), (P2), (P3), HIREARCHY 5×5, 7 SAMPLES IN PARETO FRONT)

$\mathbf{I} = [i_1 \ \cdots \ i_5]^\circ$	F	$\overline{\mathcal{C}_\mathcal{V}}$	$\overline{\mathcal{P}_\mathcal{V}}$(pW)	$\mathbf{I} = [i_1 \ \cdots \ i_5]^\circ$	F	$\overline{\mathcal{Q}_\mathcal{V}}$	$\overline{\mathcal{GD}_\mathcal{V}}$	$\mathbf{I} = [i_1 \ \cdots \ i_5]^\circ$	F	$\overline{\mathcal{C}_\mathcal{V}} \cdot \overline{\mathcal{P}_\mathcal{V}}$	$\overline{\mathcal{Q}_\mathcal{V}} / \overline{\mathcal{GD}_\mathcal{V}}$
▲27 27 27 27 27	2	.678	19.033	▶86 86 86 76 86	3	.123	14.70	▲50 27 50 27 27	0	12.070	6.08×10^{-3}
27 27 50 27 27	3	.737	18.305	76 86 76 86 86	3	.122	12.64	86 27 50 27 50	0	12.075	4.25×10^{-3}
27 27 50 27 27	4	.761	18.267	76 86 76 76 86	3	.121	12.35	86 76 86 76 86	4	12.433	3.80×10^{-3}
∗50 27 50 27 27	4	.820	17.117	76 86 50 86 76	2	.118	12.18	86 76 86 76 50	0	12.769	2.61×10^{-3}
50 27 50 50 27	4	.872	15.960	∗76 86 50 86 86	2	.117	10.71	86 76 76 76 50	0	12.939	1.79×10^{-3}
76 76 50 76 50	0	.900	15.065	27 27 27 27 27	1	.019	9.99	76 76 50 86 50	0	13.209	1.32×10^{-3}
▶76 50 50 50 27	4	.907	14.581	▼27 27 27 27 27	3	.002	6.24	▶50 27 50 27 27	4	14.044	0×10^{-3}

Fig. 12. Access coverage versus constellation hierarchy.

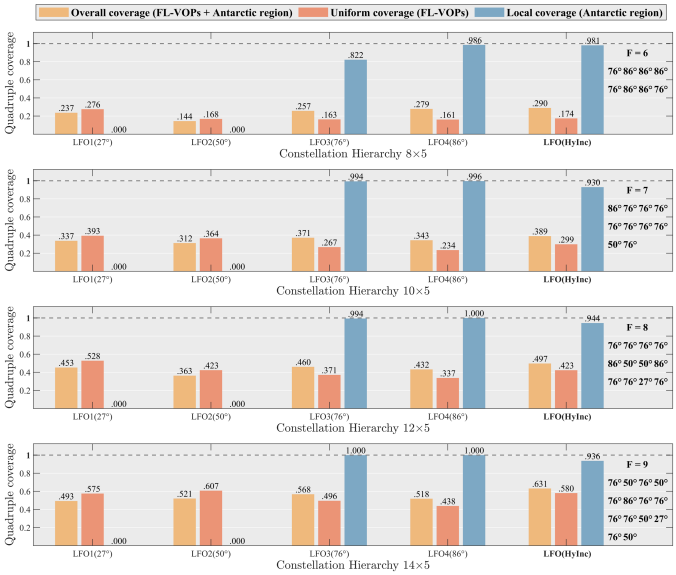

Fig. 13. Quadruple coverage versus constellation hierarchy.

GDOP tends to slow down, but the growth of the quadruple coverage performance becomes more obvious, yet it still has not exceeded 20% (in Fig. 8(a)). Thus, combining altitude to optimize navigation performance can be considered if cost is limited. For the navigation CON pursuing optimal overall navigation performance, the situation is the same as above.

B. Validation of Enhancements of the HyInc Walker

Fig. 9, Fig. 10, and Fig. 11 show a comprehensive comparison of the configurations of MOP (P1), (P2), and (P3), respectively, and the results are both fully displayed. F only needs to be regarded as an auxiliary factor in the optimization process, and the notation "$(20^\circ, 1)$" indicates $i = 20^\circ, F = 1$. Combining Fig. 9(a) and Fig. 10(a), it can be found that in the process of exchanging CON service quality for CON service quantity, the pareto-optimal solution under the HyInc Walker fits the traditional Walker in terms of inclination distribution. On the basis of this fit, since the communication CON targeting $\overline{\mathcal{C}_\mathcal{V}}$ will pursue the reduction of overlapping area, its inclination distribution gradually tends to be mid-latitude and decentralized, while the navigation CON targeting $\overline{\mathcal{Q}_\mathcal{V}}$ needs to ensure enough overlapping area, thus its inclination distribution tends to be more low-latitude and centralized. As for the LFO-based HyInc Walker, due to the destruction of the candidate inclination by orbit frozen, Fig. 9(b) and Fig. 10(b) show that the pareto optimum is forced to the original HyInc Walker's sub-optimum, which is associated with the HyInc Walker's optimum observed in Fig. 9(a),(b) and Fig. 10(a)(b).

Combined, Fig. 9, Fig. 10, and Fig. 11 show that the performance with HyInc Walker applied is all superior to that of the traditional Walker, *i.e.*, the phenomenon of weak domination in the overall sense can be observed in all of them from the function space, which is fully consistent with Lemma 1. Considering the deployable CONs, *i.e.* the frozen orbital space scenario, it can be analyzed from Fig. 9(d), Fig. 10(d), and Fig. 11(d) to know that the diversity of the pareto-optimal CONs of the traditional Walker is severely destroyed by the phenomenon of mascons, where Table III involves the pareto CONs parameters. Therefore, for an integrated CONs design for the Moon, the optionality and flexibility of the traditional Walker solution appear much poorer, and the HyInc Walker configuration is the more preferred candidate.

In addition, for Fig. 11, the pareto space designed of the CNI CON, from Fig. 11(a) and Fig. 11(b) we find that the pareto-optimal solutions in HyInc Walker all have similar inclination distributions and tend to be uniformly distributed, whereas for the case of no freezing inclination constraints, all the pareto-optimal solutions are clustered around an inclination of 10°, which is in good agreement with traditional Walker.

C. Coverage Equalization Capabilities of the HyInc Walker

In order to explore the ability of the HyInc Walker configuration to balance global uniform coverage and localized coverage enhancement in frozen orbital space, we targeted the future hotspot region of the Moon, *i.e.* the Antarctic base region [1]–[6], as a region requiring localized cover-

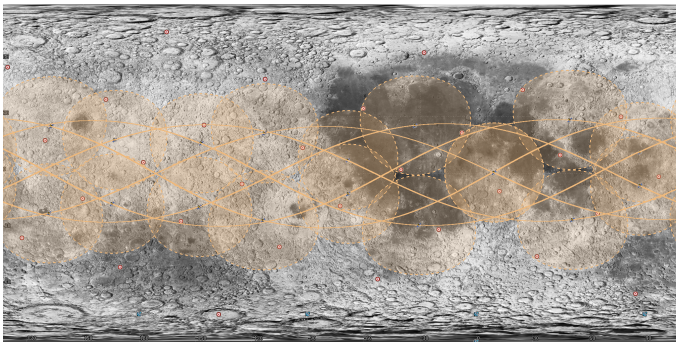

Fig. 14. Traditional Walker trajectory. ((P1), LFO1, hierarchy: 6×3)

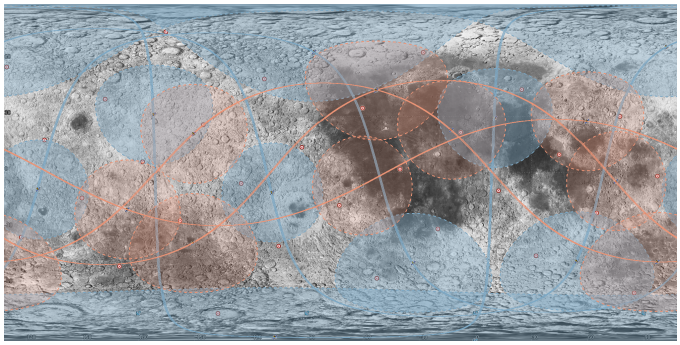

Fig. 15. HyInc Walker trajectory. ((P1), hierarchy: 6×3)

age enhancement. Specifically, we set up five VOPs near the Antarctic of the Moon, including $(90°\mathrm{S}, 0°)$, $(75°\mathrm{S}, 0°)$, $(75°\mathrm{S}, 90°\mathrm{E})$, $(75°\mathrm{S}, 180°)$, and $(75°\mathrm{S}, 90°\mathrm{W})$.

Fig. 12 and Fig. 13 respectively show the specifics of access cover and quadruple cover for different CON hierarchies ($\overline{\mathcal{C}_\mathcal{V}}$ Max and $\overline{\mathcal{Q}_\mathcal{V}}$ Max), with the data on the right side of the figures showing the specific parameters for the HyInc Walker configuration. With the increase in size, the coverage is increasing, but the growth rate is subsequently slowed down by saturation. In the traditional Walker configuration, LFO27° and LFO50° barely cover the Antarctic region, while LFO76° has better overall coverage, which is as balanced as possible between FLVOPs and the Antarctic region. On the other hand, based on LFO76°, due to the saturated coverage of the polar regions, LFO86° on the contrary weakens the uniform coverage, which in turn reduces the overall coverage.

While in the adoption of HyInc Walker configuration, the overall coverage (which is the primary target of interest and focus) is improved, and as CON size, especially the number of orbits, increases, the HyInc Walker configuration has more CON diversity and more potential space to perform, and its improvement effect before coverage saturation is also more significant. Specifically, for access coverage at the "8×3" hierarchy, compared to the 85.6% overall coverage of LFO76°, the HyInc Walker configuration reaches 92.7%, an improvement of 8.3%, where uniform coverage is enhanced by 11.9% at the cost of a 9.4% reduction in local coverage. For quadruple coverage at the "14×5" hierarchy, the HyInc Walker configuration is 63.1%, an 11% improvement compared to the 56.8% overall coverage of LFO76°, where uniform coverage is enhanced by 16.9% at the cost of a 6.4% reduction in local coverage.

The above shows that the HyInc Walker configuration has a superior coverage equalization capability. Combined with the CON trajectory diagrams in Fig. 14 and Fig. 15, the adaptive inclination and non-uniform distribution characteristics of the HyInc Walker configuration can be seen intuitively, which allows it to better optimize the utilization of CON resources.

VII. Conclusion

In this paper, we have explored pareto-optimal CNI CON design with low latency in LFO space based on the difference analysis of Earth-Moon CON construction. We have generated the global FLVOP model with Fibonnaci lattice, featuring better uniformity and stochasticity compared to LLVOP. Based on derivation of multiple objectives including access coverage, power, quadruple coverage, and GDOP, three MOPs have been proposed for better analysis and utilization of CON's overall resources. For higher practical reference value, pareto model, NSGA-II, and the construction of CON simulation system have been incorporated for the solution formation. Moreover, LFO-inspired HyInc Walker configuration has been proposed to pursue a more optimal realistic deployable integrated CON, offering superiority over traditional Walker while balancing generalizability, which has been theoretically validated and simulatively evaluated. Extensive simulation and comprehensive pareto-optimal CON analysis have been performed, such as altitude-dominated perspective of navigation performance, and the revelation of HyInc Walker's superiority in multiple scenarios including coverage equalization capability.

While excluding self-correction, inclination drift limitation can be considered to further study more practical CNI CON and applications of the proposed configuration, and more algorithms applications and comparisons could be supplementary. As a follow-up, more features revelation (*e.g.*, navigation altitude dominance mechanism, performance uncertainty range, and design rule extraction) and application studies for the proposed configuration have been organized as an interesting extension work, especially in lunar Antarctic.

Acknowledgments

The authors would like to thank the editors and anonymous reviewers for the very valuable comments received.

Appendix

Appendix A: Proof of Lemma 1

With fixed h_s, consider the $l^{th} \in \mathcal{L} = \{1, 2, ..., L\}$ CON hierarchy after factorization of M, the RAAN equalization rule of HyInc Walker represented by eq. (12) degenerates to the corresponding rule of Walker Delta, *i.e.*,

$$\begin{aligned} \Omega_\eta^{\mathscr{M}_o} = \Omega^0 + (o-1) \cdot \frac{180}{O} \cdot \left[2 - \left(\bigvee_{o=1}^{O} \left\lfloor \frac{i_o}{90} \right\rfloor \right) \right] \\ \xrightarrow{\mathfrak{x}_1} \Omega^0 + (o-1) \cdot \frac{360}{O} = \Omega_\delta^{\mathscr{M}_o}, \end{aligned} \tag{48}$$

and the corresponding degradation process to Walker Star is as follows:

$$\begin{aligned} \Omega_\eta^{\mathscr{M}_o} = \Omega^0 + (o-1) \cdot \frac{180}{O} \cdot \left[2 - \left(\bigvee_{o=1}^{O} \left\lfloor \frac{i_o}{90} \right\rfloor \right) \right] \\ \xrightarrow{\mathfrak{x}_2} \Omega^0 + (o-1) \cdot \frac{180}{O} = \Omega_\xi^{\mathscr{M}_o}, \end{aligned} \tag{49}$$

$$\mathcal{F}_{\eta}^{*}=\left\{\mathbf{\Psi}\left(\mathbf{X}_{\eta}^{*}\right)\mid\mathbf{X}_{\eta}^{*}\in\mathcal{P}_{\eta}^{*}\right\},\text{ where }\mathcal{P}_{\eta}^{*}=\{\mathbf{X}_{\eta}^{*}\mid\nexists\mathbf{X}_{\eta}:\psi_{j}\left(\mathbf{X}_{\eta}\right)\leq\psi_{j}\left(\mathbf{X}_{\eta}^{*}\right),\forall j\in\{1,2,\ldots,n\}\text{ and }\psi_{k}\left(\mathbf{X}_{\eta}\right)\leq\psi_{k}\left(\mathbf{X}_{\eta}^{*}\right),\exists k\in\{1,2,\ldots,n\}\},\mathbf{X}_{\eta}=[\mathbf{I}\ M\ O\ F],\mathbf{I}=[i_{1}\ i_{2}\ \cdots\ i_{O}],i_{o}\in[0^{\circ},90^{\circ}],\forall o\in\mathcal{O}=\{1,2,\ldots,O\}. \tag{44}$$

$$\mathcal{F}_{\tau}^{*}=\{\mathbf{\Psi}_{\tau}^{*}\mid\mathbf{\Psi}_{\tau}^{*}\in\mathcal{F}_{\delta}^{*}\cup\mathcal{F}_{\xi}^{*}\text{ and }[\nexists\mathbf{\Psi}:\psi_{j}\leq\left(\psi_{\tau}^{*}\right)_{j},\forall j\in\{1,2,\ldots,n\}\text{ and }\psi_{k}<\left(\psi_{\tau}^{*}\right)_{k},\exists k\in\{1,2,\ldots,n\}]\}. \tag{45}$$

$$\mathcal{F}_{\delta}^{*}=\{\mathbf{\Psi}\left(\mathbf{X}_{\delta}^{*}\right)\mid\mathbf{X}_{\delta}^{*}\in\mathcal{P}_{\delta}^{*}\},\text{ where }\mathcal{P}_{\delta}^{*}=\{\mathbf{X}_{\delta}^{*}\mid\nexists\mathbf{X}_{\delta}:\psi_{j}\left(\mathbf{X}_{\delta}\right)\leq\psi_{j}\left(\mathbf{X}_{\delta}^{*}\right),\forall j\in\{1,2,\ldots,n\}\text{ and }\psi_{k}\left(\mathbf{X}_{\delta}\right)\leq\psi_{k}\left(\mathbf{X}_{\delta}^{*}\right),\exists k\in\{1,2,\ldots,n\}\},\mathbf{X}_{\delta}=[i\ M\ O\ F],i\in[0^{\circ},90^{\circ}). \tag{46}$$

$$\mathcal{F}_{\xi}^{*}=\left\{\mathbf{\Psi}\left(\mathbf{X}_{\xi}^{*}\right)\mid\mathbf{X}_{\xi}^{*}\in\mathcal{P}_{\xi}^{*}\right\},\text{ where }\mathcal{P}_{\xi}^{*}=\{\mathbf{X}_{\xi}^{*}\mid\nexists\mathbf{X}_{\xi}:\psi_{j}\left(\mathbf{X}_{\xi}\right)\leq\psi_{j}\left(\mathbf{X}_{\xi}^{*}\right),\forall j\in\{1,2,\ldots,n\}\text{ and }\psi_{k}\left(\mathbf{X}_{\xi}\right)\leq\psi_{k}\left(\mathbf{X}_{\xi}^{*}\right),\exists k\in\{1,2,\ldots,n\}\},\mathbf{X}_{\xi}\overset{i\equiv90^{\circ}}{=}[M\ O\ F]. \tag{47}$$

where $\mathfrak{X}_1$ and $\mathfrak{X}_2$ denote the false and true events in eq. (13), respectively. Setting the decision spaces under HyInc Walker and Walker Delta configurations as $\mathscr{H}=\{\mathbf{X}_{\eta}\}$ and $\mathscr{D}=\{\mathbf{X}_{\delta}\}$ respectively, easily found $\mathscr{H}\supseteq\mathcal{P}_{\eta}^{*}=\{\mathbf{X}_{\eta}^{*}\},\mathscr{D}\supseteq\mathcal{P}_{\delta}^{*}=\{\mathbf{X}_{\delta}^{*}\}$, then based on the degenerate process $\mathbf{X}_{\eta}=[\mathbf{I}\ M\ O\ F]\xrightarrow[\mathfrak{Y}_1]{\mathfrak{X}_1}[i\ M\ O\ F]=\mathbf{X}_{\delta}$, where $\mathfrak{Y}_1$ denotes the event that $i_o,\forall o\in\mathcal{O}$ *equals to each other*, we can have $\mathscr{H}\supseteq\mathscr{D}$. And based on eq. (44), it is known that the union of the set of points $\mathcal{H}_j,j\in\{1,2,...,h\}$ formed by the points in the decision space $\mathscr{H}$ weakly dominated by each optimal point $\mathbf{X}_{j,\eta}^{*},j\in\{1,2,...,h\}$ in $\mathcal{P}_{\eta}^{*}=\{\mathbf{X}_{1,\eta}^{*},\mathbf{X}_{2,\eta}^{*},...,\mathbf{X}_{h,\eta}^{*}\}$ is equal to $\mathscr{H}$. Ultimately we have $\bigcup_{j=1}^{h}\mathcal{H}_j=\bigcup_{j=1}^{h}\left\{\mathbf{X}_{\eta}\mid\mathbf{X}_{j,\eta}^{*}\succeq\mathbf{X}_{\eta},\forall\mathbf{X}_{\eta}\in\mathscr{H}\right\}=\mathscr{H}\supseteq\mathscr{D}\supseteq\mathcal{P}_{\delta}^{*}$, meaning that $\mathcal{P}_{\eta}^{*}$ weakly dominates $\mathcal{P}_{\delta}^{*}$ in an overall sense and $\mathcal{F}_{\eta}^{*}$ is better than or equal to $\mathcal{F}_{\delta}^{*}$.

Similarly setting the decision space $\mathscr{S}=\{\mathbf{X}_{\xi}\}$ under the Walker Star configuration, then we have $\mathscr{S}\supseteq\mathcal{P}_{\xi}^{*}=\{\mathbf{X}_{\xi}^{*}\}$ and can obtain $\mathscr{H}\supseteq\mathscr{S}$ based on the degenerate process $\mathbf{X}_{\eta}=[\mathbf{I}\ M\ O\ F]\xrightarrow[\mathfrak{Y}_2]{\mathfrak{X}_2}[M\ O\ F]=\mathbf{X}_{\xi}$, where $\mathfrak{Y}_2$ denotes the event that $i_o=90^{\circ},\forall o\in\mathcal{O}$ and we can have $\mathscr{H}\supseteq\mathscr{S}$, followed as $\bigcup_{j=1}^{h}\mathcal{H}_j=\bigcup_{j=1}^{h}\left\{\mathbf{X}_{\eta}\mid\mathbf{X}_{j,\eta}^{*}\succeq\mathbf{X}_{\eta},\forall\mathbf{X}_{\eta}\in\mathscr{H}\right\}=\mathscr{H}\supseteq\mathscr{S}\supseteq\mathcal{P}_{\xi}^{*}$, *i.e.*, $\mathcal{P}_{\eta}^{*}$ weakly dominates $\mathcal{P}_{\xi}^{*}$ in an overall sense and $\mathcal{F}_{\eta}^{*}$ is better than or equal to $\mathcal{F}_{\xi}^{*}$.

This valid for every hierarchy $l\in\mathcal{L}=\{1,2,...,L\}$ and thus also for CON size M.

Appendix B: Proof of Lemma 2

Given $r_s=||\mathbf{v}_{\mathscr{M}}^{(t)}||_2=R_m+h_s=||\mathbf{v}_{\vartheta}^{(t)}||_2+h_s$, the SAT $\mathscr{M}$ is beyond the scope of the minimum elevation angle of VOP ϑ When $||\mathbf{d}_{\vartheta,\mathscr{M}}^{(t)}||_2^{\text{outscope}}>||\mathbf{d}_{\vartheta,\mathscr{M}}^{(t)}||_2^{\text{in-scope}}$, thus by the triangular cosine relationship $(||\mathbf{v}_{\mathscr{M}}^{(t)}||_2)^2=(||\mathbf{v}_{\vartheta}^{(t)}||_2)^2+(||\mathbf{d}_{\vartheta,\mathscr{M}}^{(t)}||_2)^2-2||\mathbf{v}_{\vartheta}^{(t)}||_2\cdot||\mathbf{d}_{\vartheta,\mathscr{M}}^{(t)}||_2\cdot\cos(\frac{\pi}{2}+\theta)$ we have $\|\mathbf{d}_{\vartheta,\mathscr{M}}\|_2^{\max}=\frac{-2\|\mathbf{v}_{\vartheta}\|_2\sin(\theta_{\min})\pm\sqrt{\left[2\|\mathbf{v}_{\vartheta}\|_2\sin(\theta_{\min})\right]^2-4\left[\left(\|\mathbf{v}_{\vartheta}\|_2\right)^2-\left(\|\mathbf{v}_{\mathscr{M}}\|_2\right)^2\right]}}{2}=-R_m\left[\sin\left(\theta_{\min}\right)\right]\pm\sqrt{R_m^2\left[\sin\left(\theta_{\min}\right)\right]^2+h_s^2+2R_mh_s}\overset{\sin(\theta_{\min})\geq0}{=}\sqrt{C_m^2+h_s^2+2R_mh_s}-C_m$. This completes the proof.

Appendix C: Proof of Lemma 3

We can have $\mathbb{E}(\boldsymbol{\varepsilon}_{\rho})=[0\ 0\ \cdots\ 0]^{\mathrm{T}}=\mathbf{0}_{M\times1}$ and a covariance relation as follows:

$$\mathbb{C}(\varepsilon_{i,\rho}\varepsilon_{j,\rho})=\begin{cases}\sigma^2,i\neq j,\\0,i=j,\end{cases}\quad\forall i,j\in[1,M], \tag{50}$$

respectively based on Assumption 1 and Assumption 2, where $\mathbb{C}(\cdot)$ denotes the covariance operator. Therefore, the covariance matrix $\mathbf{V}_{\boldsymbol{\varepsilon}_{\rho}}$ of $\boldsymbol{\varepsilon}_{\rho}$ can be obtained by

$$\mathbf{V}_{\boldsymbol{\varepsilon}_{\rho}}=\mathbb{E}\left(\left(\boldsymbol{\varepsilon}_{\rho}-\mathbb{E}\left(\boldsymbol{\varepsilon}_{\rho}\right)\right)\left(\boldsymbol{\varepsilon}_{\rho}-\mathbb{E}\left(\boldsymbol{\varepsilon}_{\rho}\right)\right)^{\mathrm{T}}\right)=\mathbb{E}\left(\boldsymbol{\varepsilon}_{\rho}\boldsymbol{\varepsilon}_{\rho}^{\mathrm{T}}\right)=\begin{bmatrix}\mathbb{V}(\varepsilon_{1,\rho})&\mathbb{C}(\varepsilon_{1,\rho}\varepsilon_{2,\rho})&\cdots&\mathbb{C}(\varepsilon_{1,\rho}\varepsilon_{M,\rho})\\\mathbb{C}(\varepsilon_{2,\rho}\varepsilon_{1,\rho})&\mathbb{V}(\varepsilon_{2,\rho})&\cdots&\mathbb{C}(\varepsilon_{2,\rho}\varepsilon_{M,\rho})\\\cdots&\cdots&\cdots&\cdots\\\mathbb{C}(\varepsilon_{M,\rho}\varepsilon_{1,\rho})&\mathbb{C}(\varepsilon_{M,\rho}\varepsilon_{2,\rho})&\cdots&\mathbb{V}(\varepsilon_{M,\rho})\end{bmatrix} \tag{51}$$

i.e. $\mathbf{V}_{\boldsymbol{\varepsilon}_{\rho}}=\sigma^2\mathbf{E}_M$, where $\mathbf{E}_M$ is the $M\times M$ unit matrix. Then the positioning error covariance matrix can be derived by

$$\mathbb{C}\left([\varepsilon_e\ \varepsilon_n\ \varepsilon_u\ \varepsilon_{\Gamma t}]\right)=\mathbb{E}\left([\varepsilon_e\ \varepsilon_n\ \varepsilon_u\ \varepsilon_{\Gamma t}]^{\mathrm{T}}\cdot[\varepsilon_e\ \varepsilon_n\ \varepsilon_u\ \varepsilon_{\Gamma t}]\right)=(\mathbf{G}^{\mathrm{T}}\mathbf{G})^{-1}\sigma^2=\mathbf{Diag}^{-}(\sigma_e^2,\sigma_n^2,\sigma_u^2,\sigma_{\Gamma t}^2). \tag{52}$$

References

[1] K. Laurini, J. Piedboeuf, B. Schade, K. Matsumoto, F. Spiero, and A. Lorenzoni, "The Global Exploration Roadmap," *IAC-11 B*, vol. 3, 2018.

[2] N. O. Harlé, S. Bywater, C. Cranstoun, J. Friend, B. Schwarz, M. Christie, and S. Sweeting, "Forward (ing) from the Moon-Lunar Pathfinder Data Relay Satellite, Paving the Way for Communication and Navigation Constellation," 2023.

[3] P. Bagla, "India Plans to Land Near Moon's South Pole," *Science*, vol. 359, no. 6375, pp. 503–504, 2018.

[4] Y. Wei, Z. Yao, and W. Wan, "China's Roadmap for Planetary Exploration," *Nature Astronomy*, vol. 2, no. 5, pp. 346–348, 2018.

[5] C. Li, C. Wang, Y. Wei, and Y. Lin, "China's Present and Future Lunar Exploration Program," *Science*, vol. 365, no. 6450, pp. 238–239, 2019.

[6] M. Wei, C. Hu, D. Estévez, M. Tai, Y. Zhao, J. Huang, C. Bassa, T. Jan Dijkema, X. Cao, and F. Wang, "Design and Flight Results of the VHF/UHF Communication System of Longjiang Lunar Microsatellites," *Nature communications*, vol. 11, no. 1, p. 3425, 2020.

[7] M. Y. Abdelsadek, A. U. Chaudhry, T. Darwish, E. Erdogan, G. Karabulut-Kurt, P. G. Madoery, O. B. Yahia, and H. Yanikomeroglu, "Future Space Networks: Toward the Next Giant Leap for Humankind," *IEEE Trans. Commun.*, vol. 71, no. 2, pp. 949–1007, 2022.

[8] M. Werner, A. Jahn, E. Lutz, and A. Bottcher, "Analysis of System Parameters for LEO/ICO-satellite Communication Networks," *IEEE J. Sel. Areas Commun.*, vol. 13, no. 2, pp. 371–381, 1995.

[9] H. Guo, J. Li, J. Liu, N. Tian, and N. Kato, "A Survey on Space-Air-Ground-Sea Integrated Network Security in 6G," *IEEE Commun. Surv. Tutor.*, vol. 24, no. 1, pp. 53–87, 2021.

[10] S. Liu, Z. Gao, Y. Wu, D. W. K. Ng, X. Gao, K.-K. Wong, S. Chatzinotas, and B. Ottersten, "LEO Satellite Constellations for 5G and Beyond: How Will They Reshape Vertical Domains?" *IEEE Commun. Mag.*, vol. 59, no. 7, pp. 30–36, 2021.

[11] A. Al-Hourani, "Session Duration between Handovers in Dense LEO Satellite Networks," *IEEE Wirel. Commun. Lett.*, vol. 10, no. 12, pp. 2810–2814, 2021.

[12] Y. Su, Y. Liu, Y. Zhou, J. Yuan, H. Cao, and J. Shi, "Broadband LEO Satellite Communications: Architectures and Key Technologies," *IEEE Wirel. Commun.*, vol. 26, no. 2, pp. 55–61, 2019.

[13] B. Al Homssi, A. Al-Hourani, K. Wang, P. Conder, S. Kandeepan, J. Choi, B. Allen, and B. Moores, "Next Generation Mega Satellite Networks for Access Equality: Opportunities, Challenges, and Performance," *IEEE Commun. Mag.*, vol. 60, no. 4, pp. 18–24, 2022.

[14] P. Wang, B. Di, and L. Song, "Mega-constellation Design for Integrated Satellite-Terrestrial Networks for Global Seamless Connectivity," *IEEE Wirel. Commun. Lett.*, vol. 11, no. 8, pp. 1669–1673, 2022.

[15] R. Deng, B. Di, H. Zhang, L. Kuang, and L. Song, "Ultra-dense LEO Satellite Constellations: How Many LEO Satellites Do We Need?" *IEEE Trans. Wirel. Commun.*, vol. 20, no. 8, pp. 4843–4857, 2021.

[16] B. Di, L. Song, Y. Li, and H. V. Poor, "Ultra-dense LEO: Integration of Satellite Access Networks into 5G and Beyond," *IEEE Wirel. Commun.*, vol. 26, no. 2, pp. 62–69, 2019.

[17] Z. Zhang, Y. Li, C. Huang, Q. Guo, L. Liu, C. Yuen, and Y. L. Guan, "User Activity Detection and Channel Estimation for Grant-free Random Access in LEO Satellite-enabled Internet of Things," *IEEE Internet Things J.*, vol. 7, no. 9, pp. 8811–8825, 2020.

[18] P. Wang, B. Di, and L. Song, "Multi-layer LEO Satellite Constellation Design for Seamless Global Coverage," in *2021 IEEE Global Communications Conference (GLOBECOM)*. IEEE, 2021, pp. 01–06.

[19] G. Zeng, Y. Zhan, H. Xie, and C. Jiang, "Resource Allocation for Networked Telemetry System of Mega LEO Satellite Constellations," *IEEE Trans. Commun.*, vol. 70, no. 12, pp. 8215–8228, 2022.

[20] R. Deng, B. Di, S. Chen, S. Sun, and L. Song, "Ultra-dense LEO Satellite Offloading for Terrestrial Networks: How Much to Pay the Satellite Operator?" *IEEE Trans. Wirel. Commun.*, vol. 19, no. 10, pp. 6240–6254, 2020.

[21] H. Jia, Z. Ni, C. Jiang, L. Kuang, and J. Lu, "Uplink Interference and Performance Analysis for Megasatellite Constellation," *IEEE Internet Things J.*, vol. 9, no. 6, pp. 4318–4329, 2021.

[22] B. Al Homssi and A. Al-Hourani, "Modeling Uplink Coverage Performance in Hybrid Satellite-Terrestrial Networks," *IEEE Commun. Lett.*, vol. 25, no. 10, pp. 3239–3243, 2021.

[23] S. Ji, D. Zhou, M. Sheng, and J. Li, "Mega Satellite Constellation System Optimization: From a Network Control Structure Perspective," *IEEE Trans. Wirel. Commun.*, vol. 21, no. 2, pp. 913–927, 2021.

[24] X. Wang and S. Zhang, "Cost Analysis for Mass Customized Production of Satellites based on Modularity," *IEEE Access*, vol. 9, pp. 13 754–13 760, 2021.

[25] F. Pereira and D. Selva, "Exploring the Design Space of Lunar GNSS in Frozen Orbit Conditions," in *2020 IEEE/ION Position, Location and Navigation Symposium (PLANS)*. IEEE, 2020, pp. 444–451.

[26] G. M. Capez, S. Henn, J. A. Fraire, and R. Garello, "Sparse Satellite Constellation Design for Global and Regional Direct-to-Satellite IoT Services," *IEEE Trans. Aerosp. Electron. Syst.*, vol. 58, no. 5, pp. 3786–3801, 2022.

[27] C. Dai, G. Zheng, and Q. Chen, "Satellite Constellation Design with Multi-objective Genetic Algorithm for Regional Terrestrial Satellite Network," *China Commun.*, vol. 15, no. 8, pp. 1–10, 2018.

[28] J. Jiang, S. Yan, and M. Peng, "Regional LEO Satellite Constellation Design Based on User Requirements," in *2018 IEEE/CIC International Conference on Communications in China (ICCC)*. IEEE, 2018, pp. 855–860.

[29] Y. Wei, H. Li, and X. Du, "An Efficient LEO Global Navigation Constellation Design Based on Walker Constellation," in *2020 IEEE Computing, Communications and IoT Applications (ComComAp)*. IEEE, 2020, pp. 1–6.

[30] X. Xu, Z. Ju, and J. Luo, "Design of Constellations for GNSS Reflectometry Mission Using the Multiobjective Evolutionary Algorithms," *IEEE Trans. Geosci. Remote Sensing*, vol. 60, pp. 1–15, 2022.

[31] R. Luo, H. Yuan, and Y. Xu, "Navigation Augmentation based on LEO Communication Satellite Constellations," in *Proceedings of the 2018 International Technical Meeting of The Institute of Navigation*, 2018, pp. 188–195.

[32] N. Witternigg, G. Obertaxer, M. Schönhuber, G. B. Palmerini, F. Rodriguez, L. Capponi, F. Soualle, and J.-J. Floch, "Weak GNSS Signal Navigation for Lunar Exploration Missions," in *Proceedings of the 28th International Technical Meeting of the Satellite Division of The Institute of Navigation (ION GNSS+ 2015)*, 2015, pp. 3928–3944.

[33] F. Pereira, P. M. Reed, and D. Selva, "Multi-objective Design of a Lunar GNSS," *Navig. J. Inst. Navig.*, vol. 69, no. 1, 2022.

[34] F. Pereira and D. Selva, "Analysis of Navigation Performance with Lunar GNSS Evolution," in *Proceedings of the 2022 International Technical Meeting of The Institute of Navigation*, 2022, pp. 514–529.

[35] M. Murata, I. Kawano, and S. Kogure, "Lunar Navigation Satellite System and Positioning Accuracy Evaluation," in *Proceedings of the 2022 International Technical Meeting of The Institute of Navigation*, 2022, pp. 582–586.

[36] M. Murata, K. Akiyama, and N. Satoh, "Lunar South Pole Region Navigation Using Lunar Navigation Satellite System," in *Proceedings of the 36th International Technical Meeting of the Satellite Division of The Institute of Navigation (ION GNSS+ 2023)*, 2023, pp. 3589–3596.

[37] S. Bhamidipati, T. Mina, and G. Gao, "Time Transfer from GPS for Designing a SmallSat-based Lunar Navigation Satellite System," *Navig. J. Inst. Navig.*, vol. 69, no. 3, 2022.

[38] ——, "A Case Study Analysis for Designing a Lunar Navigation Satellite System with Time Transfer from the Earth GPS," *Navig. J. Inst. Navig.*, vol. 70, no. 4, 2023.

[39] L. Yin, Q. Ni, and Z. Deng, "A GNSS/5G Integrated Positioning Methodology in D2D Communication Networks," *IEEE J. Sel. Areas Commun.*, vol. 36, no. 2, pp. 351–362, 2018.

[40] G. Zanotti, M. Ceresoli, A. Pasquale, J. Prinetto, and M. Lavagna, "High performance lunar constellation for navigation services to moon orbiting users," *Adv. Space Res.*, 2023.

[41] C.-Q. Dai, M. Zhang, C. Li, J. Zhao, and Q. Chen, "QoE-aware Intelligent Satellite Constellation Design in Satellite Internet of Things," *IEEE Internet Things J.*, vol. 8, no. 6, pp. 4855–4867, 2020.

[42] W.-Q. Wang and D. Jiang, "Integrated Wireless Sensor Systems via Near-Space and Satellite Platforms: A Review," *IEEE Sens. J.*, vol. 14, no. 11, pp. 3903–3914, 2014.

[43] J. Thompson, H. Haygood, and M. Kezirian, "Design and Analysis of Lunar Communication and Navigation Satellite Constellation Architectures," in *AIAA SPACE 2010 Conference & Exposition*, 2010, p. 8644.

[44] A. Grenier, P. Giordano, L. Bucci, A. Cropp, P. Zoccarato, R. Swinden, and J. Ventura-Traveset, "Positioning and Velocity Performance Levels for a Lunar Lander Using a Dedicated Lunar Communication and Navigation System," *Navig. J. Inst. Navig.*, vol. 69, no. 2, 2022.

[45] S. Bhamidipati, T. Mina, A. Sanchez, and G. Gao, "A lunar Navigation and Communication Satellite System with Earth-GPS Time Transfer: Design and Performance Considerations," in *Proceedings of the 35th International Technical Meeting of the Satellite Division of The Institute of Navigation (ION GNSS+ 2022)*, 2022, pp. 537–553.

[46] ——, "Satellite Constellation Design for a Lunar Navigation and Communication System," *Navig. J. Inst. Navig.*, vol. 70, no. 4, 2023.

[47] C.-J. Wang, "Structural Properties of a Low Earth Orbit Satellite Constellation-the Walker delta Network," in *Proceedings of MILCOM'93-IEEE Military Communications Conference*, vol. 3. IEEE, 1993, pp. 968–972.

[48] D. Mortari and M. P. Wilkins, "Flower Constellation Set Theory. Part I: Compatibility and Phasing," *IEEE Trans. Aerosp. Electron. Syst.*, vol. 44, no. 3, pp. 953–962, 2008.

[49] M. E. Avendano and D. Mortari, "New Insights on Flower Constellations Theory," *IEEE Trans. Aerosp. Electron. Syst.*, vol. 48, no. 2, pp. 1018–1030, 2012.

[50] N. Okati, T. Riihonen, D. Korpi, I. Angervuori, and R. Wichman, "Downlink Coverage and Rate Analysis of Low Earth Orbit Satellite Constellations Using Stochastic Geometry," *IEEE Trans. Commun.*, vol. 68, no. 8, pp. 5120–5134, 2020.

[51] M. E. Muller, "A Note on a Method for Generating Points Uniformly on N-Dimensional Spheres," *Commun. ACM*, vol. 2, no. 4, pp. 19–20, 1959.

[52] Á. González, "Measurement of Areas on a Sphere Using Fibonacci and Latitude–Longitude lattices," *Math Geosci.*, vol. 42, pp. 49–64, 2010.

[53] A. Konopliv, A. Binder, L. Hood, A. Kucinskas, W. Sjogren, and J. Williams, "Improved Gravity Field of the Moon from Lunar Prospector," *Science*, vol. 281, no. 5382, pp. 1476–1480, 1998.

[54] M. T. Zuber, D. E. Smith, M. M. Watkins, S. W. Asmar, A. S. Konopliv, F. G. Lemoine, H. J. Melosh, G. A. Neumann, R. J. Phillips, S. C. Solomon *et al.*, "Gravity Field of the Moon from the Gravity Recovery and Interior Laboratory (GRAIL) Mission," *Science*, vol. 339, no. 6120, pp. 668–671, 2013.

[55] G. A. Neumann, M. T. Zuber, M. A. Wieczorek, J. W. Head, D. M. Baker, S. C. Solomon, D. E. Smith, F. G. Lemoine, E. Mazarico, T. J. Sabaka *et al.*, "Lunar Impact Basins Revealed by Gravity Recovery and Interior Laboratory Measurements," *Sci. Adv.*, vol. 1, no. 9, p. e1500852, 2015.

[56] D. Gaur and M. S. Prasad, "Communication Relay Satellites Constellation Assessment for Future Lunar Missions," in *2020 8th International Conference on Reliability, Infocom Technologies and Optimization (Trends and Future Directions)(ICRITO)*. IEEE, 2020, pp. 1195–1200.

[57] K. Deb, A. Pratap, S. Agarwal, and T. Meyarivan, "A Fast and Elitist Multiobjective Genetic Algorithm: NSGA-II," *IEEE Trans. Evol. Comput.*, vol. 6, no. 2, pp. 182–197, 2002.

[58] F. Causa and G. Fasano, "Improving Navigation in GNSS-challenging Environments: Multi-UAS Cooperation and Generalized Dilution of Precision," *IEEE Trans. Aerosp. Electron. Syst.*, vol. 57, no. 3, pp. 1462–1479, 2020.
[59] B. Huang, Z. Yao, X. Cui, and M. Lu, "Dilution of Precision Analysis for GNSS Collaborative Positioning," *IEEE Trans. Veh. Technol.*, vol. 65, no. 5, pp. 3401–3415, 2015.
[60] E. D. Kaplan and C. Hegarty, *Understanding GPS/GNSS: Principles and Applications*. Artech house, 2017.
[61] V. S. I. Dutt, G. S. B. Rao, S. S. Rani, S. R. Babu, R. Goswami, and C. U. Kumari, "Investigation of GDOP for Precise User Position Computation with All Satellites in View and Optimum Four Satellite Configurations," *J. Ind. Geophys. Union*, vol. 13, no. 3, pp. 139–148, 2009.
[62] P. Gao, L. Lian, and J. Yu, "Cooperative ISAC with Direct Localization and Rate-Splitting Multiple Access Communication: A Pareto Optimization Framework," *IEEE J. Sel. Areas Commun.*, vol. 41, no. 5, pp. 1496–1515, 2023.
[63] H. Lee, S. H. Lee, and T. Q. Quek, "MOSAIC: Multiobjective Optimization Strategy for AI-Aided Internet of Things Communications," *IEEE Internet Things J.*, vol. 9, no. 17, pp. 15 657–15 673, 2022.
[64] G. Amendola, D. Cavallo, T. Chaloun, N. Defrance, G. Goussetis, M. Margalef-Rovira, E. Martini, O. Quevedo-Teruel, V. Valenta, N. J. Fonseca *et al.*, "Low-Earth Orbit User Segment in the Ku and Ka-Band: An Overview of Antennas and RF Front-End Technologies," *IEEE Microw. Mag.*, vol. 24, no. 2, pp. 32–48, 2023.

Guoquan Chen (Graduate Student Member, IEEE) received the B.E. degree in electronic and information engineering from the Harbin Institute of Technology (Shenzhen) in 2022, where he is currently pursuing the M.S. degree with the Department of Electronic Engineering. His research interests include aerospace communications and networks, satellite constellation design, and wireless communications and networks. He has been a Session Chair of the IEEE Globecom and a TPC Member of the IEEE Wireless Communications and Networking Conference.

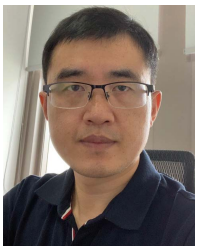

Shaohua Wu (Member, IEEE) received the Ph.D. degree in communication engineering from the Harbin Institute of Technology in 2009. From 2009 to 2011, he held a post-doctoral position at the Department of Electronics and Information Engineering, Shenzhen Graduate School, Harbin Institute of Technology, where he has been with since 2012. From 2014 to 2015, he was a Visiting Researcher with BBCR, University of Waterloo, Canada. He is currently a Full Professor with the Harbin Institute of Technology (Shenzhen), China. He is also a Professor with the Peng Cheng Laboratory, Shenzhen, China. His research interests include satellite and space communications, advanced channel coding techniques, space-air-ground-sea integrated networks, and B5G/6G wireless transmission technologies. He has authored or coauthored over 100 papers in these fields and holds over 40 Chinese patents.

Junhua You received the B.E. degree in electronic and information engineering from the Harbin Institute of Technology (Shenzhen) in 2021, where he is currently pursuing the Ph.D. degree with the Department of Electronic Engineering. His research interests include satellite communications, advanced channel coding, and timely transmission.

Qinyu Zhang (Senior Member, IEEE) received the bachelor's degree in communication engineering from the Harbin Institute of Technology (HIT), Harbin, China, in 1994, and the Ph.D. degree in biomedical and electrical engineering from the University of Tokushima, Tokushima, Japan, in 2003. From 1999 to 2003, he was an Assistant Professor with the University of Tokushima. From 2003 to 2005, he was an Associate Professor with the Shenzhen Graduate School, HIT, and the Founding Director at the Communication Engineering Research Center, School of Electronic and Information Engineering (EIE). Since 2005, he has been a Full Professor and the Dean of the EIE School, HIT. His research interests include aerospace communications and networks, wireless communications and networks, cognitive radios, signal processing, and biomedical engineering. He has been a TPC Member of the Infocom, IEEE ICC, IEEE Globecom, IEEE Wireless Communications and Networking Conference, and other flagship conferences in communications. He was an Associate Chair of Finance of the International Conference on Materials and Manufacturing Technologies 2012, the TPC Co-Chair of the IEEE/CIC ICCC 2015, and the Symposium Co-Chair of the CHINACOM 2011 and the IEEE Vehicular Technology Conference 2016 (Spring). He was the Founding Chair of the IEEE Communications Society Shenzhen Chapter. He is on the Editorial Board of some academic journals, such as *Journal of Communication*, *KSII Transactions on Internet and Information Systems*, and *Science China Information Sciences*.